Experimental study of the Zeeman splitting of boron levels in silicon

F. Merlet, B. Pajot, Ph. Arcas, and A. M. Jean-Louis

Laboratoire d'Infrarouge, Laboratoire Associé au Centre National de la Recherche Scientifique, Université de Paris VI, Bâtiment 350, 91405 Orsay, France

(Received 23 December 1974)

The Zeeman effect of the first four photoexcitation lines of boron in silicon has been investigated in crystals with low boron concentration ($\sim 10^{14}$ atoms/cm^3) and for magnetic fields up to 64 kG with $\vec{E} \perp \vec{B}$ and $\vec{E} \| \vec{B}$. As many as eleven discrete components have been resolved for line 1 for $\vec{B}_{\|} \langle 100 \rangle$. No quadratic shift is observed for lines 1 and 2, but a small interaction is found between the excited sublevels of line 3 and other excited sublevels. Line 4 exhibits a characteristic upwards shift which can be fitted for most components to a quadratic law. By comparison with behavior of boron in germanium, it is found that the observed splitting is mainly due to the splitting of the ground state, which is about twice that of the excited states and this accounts for the thermalization effect observed at high fields. The results can be explained by assuming for the excited states of lines 1 and 2 the Γ_8 symmetry as deduced from piezospectroscopic measurements. The symmetry of the excited state of line 3 cannot be obtained with certainty from our experimental results and the data for line 4 can be partially explained on the basis of a $\Gamma_6 + \Gamma_7$ symmetry. With the assumption of a symmetric splitting of the ground state, it has been found that the splitting of the excited states of line 1 is asymmetric and anisotropic, in contrast to the corresponding splitting for line 2. The g factors obtained for the ground state are in qualitative agreement with the experimental determinations by magneto-Raman effect. The results obtained for the excited states of lines 1 and 2 are quantitatively self-consistent with respect to the anisotropy of the g factors and to the selection rules given by Bhattacharjee and Rodriguez. It has also been possible to estimate for line 1 the parameters u and v governing the relative intensities of the allowed transitions. A comparison with theory for line 4 shows its partial breakdown due to the failure to meet the prerequisite for group-theoretical analysis.

I. INTRODUCTION

Various attempts have been made to obtain a reasonable understanding of the excited levels of the acceptor impurities in group-IV semiconductors,[1-5] comparable for instance with that of the excited levels of the donor impurities in these materials.[6] For germanium, the agreement between theory and experiment seems now to be satisfactory, at least for the first excited levels, but this is not the case for silicon since the infrared excitation lines observed cannot be ascribed with certainty to specific transitions by mere comparison between theoretical and experimental spacings.

Absorption and scattering experiments under an external perturbation have provided valuable information on the nature of the acceptor states. Piezospectroscopic studies of acceptors in silicon and germanium have yielded the symmetry of the states involved, together with their deformation potentials.[7,8] The Zeeman effect of group-III impurities in silicon was first reported by Zwerdling *et al.*[9,10] and it showed, on the main, a complex behavior. A similar study of double acceptors in germanium has also been reported by Moore.[11] More recently a detailed investigation of the splitting of the excitation spectrum of boron and thallium in germanium[12] has provided the g factors of the ground and of some excited states, which can be compared with the theoretical predictions.[13,14] The g factor under stress of the ground state of acceptor impurities in silicon has been investigated by Feher *et al.* using paramagnetic-resonance techniques.[15] Their value for boron is higher than that found by Cherlow *et al.*[16] in a study of the magneto-Raman effect of the Raman-active boron transition in silicon, and the discrepancy is not yet explained.

II. THEORY

The description of the acceptor levels in silicon and germanium using the effective-mass approximation (EMA) is closely related to the structure of the valence band of these materials at zero wave vector. It consists of two degenerate upper bands labeled by the irreducible representation Γ_8^+ of the double point group $\bar{O}_h$ and a band with irreducible representation Γ_7^+, separated from the two upper ones by a spin-orbit splitting of about 44 meV for silicon.[10] One can observe in fact two series of impurity transitions: those between the ground state associated with the Γ_8^+ valence band and the corresponding excited states ($p_{3/2}$ series) and those between the same ground state and the excited states associated with the Γ_7^+ valence band ($p_{1/2}$ series). The $p_{1/2}$ excitation spectrum first observed by Zwerdling *et al.*,[10] who studied its Zeeman effect in boron and aluminum-doped silicon, consists of two lines, $2p'$ and $3p'$. The lines of the $p_{3/2}$ series of boron in silicon have been labeled 1, 2, 3, etc., in order of increasing energy

gy.[17] This convention has been extended henceforth to the group-III impurities in silicon with minor additions (lines 4*A* and 4*B*).

The calculation of the energy of the acceptor levels in silicon and germanium was first worked out by Schetcher[2] in the framework of the EMA. From group-theoretical considerations, he showed that, by analogy with atomic spectroscopy, s-like states of the Γ_8^+ valence band transformed under the fourfold irreducible representation Γ_8 of $\overline{T}_d$, while the p-like states transformed under the irreducible representations Γ_6, Γ_7, and Γ_8 of $\overline{T}_d$. Under a perturbation which is antisymmetric with respect to the time-reversal operator, a $\Gamma_8(j=\frac{3}{2})$ level splits into a quarted with $m_j=\frac{3}{2}$, $\frac{1}{2}$, $-\frac{1}{2}$, and $-\frac{3}{2}$, the Γ_6 and Γ_7 levels into a doublet with $m_j=\frac{1}{2}$ and $-\frac{1}{2}$. In the absence of any quadratic effect, the g factors of an unperturbed level which splits into components of energy $E_j^{(m_j)}$ in a magnetic field of magnitude B are given by

$$g_j^{(m_j)}=(E_j^{(m_j)}-E_j)/\mu_B m_j B\ .$$

E_j is the zero-field position of the level, μ_B is the Bohr magneton, and $g_{m_j}=-g_{-m_j}$ (we will subsequently drop the index j as we will be concerned, unless otherwise specified, with $j=\frac{3}{2}$ levels).

Regardless of the proper Hamiltonian of the particle, the case of the spin Hamiltonian for a Γ_8 state has been treated by Bleaney.[18] This Hamiltonian can be expressed in terms of two parameters g_1' and g_2' which have been substituted for g and f, respectively, in the original paper:

$$H_{\text{Zee}}=\mu_B[g_1'\,\vec{J}\cdot\vec{B}+g_2'(J_x^3B_x+J_y^3B_y+J_z^3B_z)]\ ,$$

where $\vec{J}$ is the total angular momentum instead of the spin $\vec{S}$. Yafet and Thomas[19] have reexpressed Bleaney's results in terms of an average g factor M and a parameter ϵ describing the deviation from spherical symmetry. (The parameters K and L used by these authors are identical with g_1' and g_2', respectively.) By introducing $r=g_2'/4g_1'$, one obtains for the expressions for the positive g factors of the outer (o) and inner (i) sublevels of a Γ_8 level split by the magnetic field

$$9g_o^2=g_1'^2(5\gamma+4\alpha\{\gamma+\beta[1-15(l^2m^2+m^2n^2+n^2l^2-\tfrac{1}{5})]\}^{1/2}),$$

$$g_i^2=g_1'^2(5\gamma-4\alpha\{\gamma+\beta[1-15(l^2m^2+m^2n^2+n^2l^2-\tfrac{1}{5})]\}^{1/2}),$$

where $\alpha=1+7r$, $\beta=12r(1+10r)/5$, and $\gamma=\alpha^2+\beta$; l, m, n are the direction cosines of the applied magnetic field. The identification gives $M^2=\gamma g_1'^2$, $\epsilon=-\beta/\gamma$, and $g_o(100)g_i(100)=g_1'^2(3\alpha^2-5\beta)$. The parameter r describes also the deviation from spherical symmetry since for $r=0$, $\beta=0$ and $\alpha=\gamma=1$. The outer levels can correspond either to $m_j=\pm\frac{3}{2}$ or to $m_j=\pm\frac{1}{2}$. Since the Hamiltonian is unchanged when the states with $m_j=\frac{3}{2}$, $\frac{1}{2}$, $-\frac{1}{2}$, and $-\frac{3}{2}$ undergo a cyclic permutation leading to $m_j=-\frac{1}{2}$, $-\frac{3}{2}$, $\frac{3}{2}$, and $\frac{1}{2}$, the situation is left the same provided new values of the parameters are used,[18] namely,

$$3g_1'=-G_1(10+91R)$$

$$r=-\frac{1+10R}{10+91R}\ .$$

From the above results, it is clear that, for r given, the outer levels cannot cross the inner levels when the orientation of the magnetic field is changed. This limits r to 0 or to lie within the range $-\frac{1}{13}$ to $-\frac{1}{8}$. For $r=-\frac{1}{13}$, $3g_o(100)=g_i(100)$, and for $r=-\frac{1}{8}$, $g_i(100)=0$. It has also been noted by Cherlow *et al.*[16] that the splitting is identical when the magnetic field is parallel either to a $\langle 011\rangle$ or to a $\langle 211\rangle$ direction; this arises from the invariance of $l^2m^2+m^2n^2+n^2l^2$ in the two cases.

A group-theoretical treatment of the splitting of the acceptor levels in a tetrahedral site has been undertaken by Bhattacharjee and Rodriguez[20] when the magnetic field is parallel to a $\langle 100\rangle$, $\langle 111\rangle$, or $\langle 011\rangle$ direction: For the Γ_6 and Γ_7 levels, the splitting is isotropic. It is given by

$$E_{\pm 1/2}^{(k)}=\pm\,\mu_B g_k B/2+q_k B^2\ ,$$

with $k=6$ or 7; q determines the quadratic shift of the levels. For a Γ_8 level, the expressions for the linear part of the g factors are given below

$$g_{3/2}(100)=g_1'(1+9r)\ ,$$

$$g_{1/2}(100)=g_1'(1+r)\ ,$$

$$3g_{3/2}(111)=g_1'r[(3/r+23)^2+32]^{1/2}\ ,$$

$$g_{1/2}(111)=g_1'(1+13r)\ ,$$

$$3g_{3/2}(110)=g_1'[1+r(8\Delta+7)]\ ,$$

$$g_{1/2}(110)=g_1'[r(8\Delta-7)-1]\ ,$$

with $8\Delta=[(17+2/r)^2+27]^{1/2}$.

When r is positive, $g_{3/2}$ and $g_{1/2}$ have the same sign as g_1' with $|g_{3/2}|>|g_{1/2}|$. When $r=0$, the splitting is isotropic and the levels are uniformly spaced ($g_{3/2}=g_{1/2}=g_1'$). The situation where r is negative is summarized in Table I.

The selection rules are deduced from symmetry considerations alone and they are given in Table II. The relative intensities of the Zeeman components have been reexpressed in terms of the dipole matrix elements of the unperturbed wave functions, by introducing, in the case of a $\Gamma_8-\Gamma_8$ transition the parameters D and D'. For $\vec{B}\parallel\langle 100\rangle$, the sum of the transition probabilities for the various transitions is given by

$$N=4|D+D'|^2+16|D'|^2\ ,$$

which allows the normalization of the transition probability for the zero-field transition. The parameters u and v are then defined by

TABLE I. Anisotropy of the splitting of a $j=\frac{3}{2}$ level as a function of r and of the orientation of the magnetic field; r and g_1' are supposed to be negative.

r	$\vec{B}\parallel\langle 100\rangle$	$\vec{B}\parallel\langle 111\rangle$	$\vec{B}\parallel\langle 011\rangle$
	$r>-\frac{1}{9}$ $g_{3/2}$ and $g_{1/2}<0$	$3g_{3/2}>\lvert g_{1/2}\rvert$	$g_{3/2}$ and $g_{1/2}>0$
	$r>-\frac{1}{13}$ $3g_{3/2}<g_{1/2}$	$r>-\frac{1}{13}$ $g_{1/2}<0$	$r>-\frac{1}{7}$ $3g_{3/2}<g_{1/2}$
$-\frac{1}{13}$	$3g_{3/2}=g_{1/2}=12g_1'/13$	$g_{3/2}=-4g_1'\sqrt{2}/13$ $g_{1/2}=0$	$g_{3/2}=-2g_1'(\sqrt{3}-1)/13$ $g_{1/2}=-6g_1'(\sqrt{3}+1)/13$
	$-\frac{1}{9}<r<-\frac{1}{8}$ $3g_{3/2}>g_{1/2}$	$r<-\frac{1}{13}$ $g_{1/2}>0$	
$-\frac{1}{10}$	$g_{3/2}=g_1'/10$ $g_{1/2}=9g_1'/10$	$g_{3/2}=g_{1/2}=-3g_1'/10$	$g_{3/2}=-g_1'/10$ $g_{1/2}=-9g_1'/10$
$-\frac{1}{9}$	$g_{3/2}=0$ $g_{1/2}=8g_1'/9$	$g_{3/2}=-4g_1'/9\sqrt{3}$ $g_{1/2}=-4g_1'/9$	$3g_{3/2}=-2g_1'(\sqrt{7}-1)/9$ $g_{1/2}=-2g_1'(\sqrt{7}+1)/9$
	$-1<r<-\frac{1}{9}$ $g_{3/2}>0$ $g_{1/2}<0$		
	$-\frac{1}{7}<r<\frac{1}{9}$ $3g_{3/2}<\lvert g_{1/2}\rvert$		
$-\frac{1}{7}$	$3g_{3/2}=\lvert g_{1/2}\rvert=-6g_1'/7$	$3g_{3/2}=g_{1/2}=-6g_1'/7$	$3g_{3/2}=g_{1/2}=-6g_1'/7$
	$-1<r<-\frac{1}{7}$ $3g_{3/2}>\lvert g_{1/2}\rvert$		$r<-\frac{1}{7}$ $3g_{3/2}>g_{1/2}$
-1	$g_{3/2}=-8g_1'$ $g_{1/2}=0$		
	$r<-1$ $g_{3/2}$ and $g_{1/2}>0$		

$$|D+D'|^2=N(1-u)/4\ ,$$

$$|D|^2=N(1-3u/4+v)/4\ .$$

When $\vec{B}$ is parallel to a $\langle 100\rangle$ direction, the relative intensities of the allowed transitions can be expressed as functions of only u and v; for $\vec{B}\parallel\langle 111\rangle$ or $\vec{B}\parallel\langle 011\rangle$, it has been shown that they depend also on the ratio of the g factors g_1' and g_2'. When $\vec{E}\perp\vec{B}\parallel[110]$, the relative intensities depend also on the orientation of $\vec{E}$ in the plane (110). The expressions for $\vec{E}\parallel[\bar{1}10]$ and $\vec{E}\parallel[001]$, i.e., $\vec{k}\parallel[001]$ and $\vec{k}\parallel[\bar{1}10]$, respectively, in the transverse configuration can be found in Ref. 20. The formulation of Yafet and Thomas is of course equivalent to that of Bhattacharjee and Rodriguez as long as we consider the magnitude of the splitting of a $\Gamma_8(\frac{3}{2})$ level as a function of the orientation of the magnetic field, but we see for instance that for $g_1'<0$ and $r=-\frac{1}{10}$, a sublevel with $m_j=-\frac{3}{2}$ when $\vec{B}\parallel\langle 100\rangle$ transforms into a state with $m_j=\frac{1}{2}$ when $\vec{B}\parallel\langle 111\rangle$ and into a state with $m_j=\frac{3}{2}$ when $\vec{B}\parallel\langle 011\rangle$. This can be qualitatively understood if we assume that for a random orientation of the magnetic field, m_j is not a good quantum number and that a sublevel can be described by a linear combination of states with definite m_j values, which reduce to one component only for specific orientations of the magnetic field.

It must be noted that the full validity of the above results requires the Zeeman splitting of a level to be small in comparison with its distance from the nearest zero-field level, which is strictly the case neither in silicon nor in germanium but they can be very useful as long as we do not want quantitative comparisons.

On the other hand, quantum-mechanical calculations of the g factors using perturbation theory within the EMA have been undertaken for $\vec{B}\parallel\langle 100\rangle$ by Lin Chung and Wallis for germanium[14] and by Suzuki *et al.* for germanium and silicon.[13] They have obtained numerical values of the matrix elements

$$\langle F^{(m_j)}|H_{\text{Zee}}|F^{(m_j)}\rangle=E_j^{(m_j)}-E_j\ ,$$

where the $F^{(m_j)}$'s are the multidimensional-envelope wave functions of the EMA. They obtain for the ground state of the substitutional acceptor

TABLE II. Selection rules for the transitions originating from a Γ_8 quartet to a Γ_8 quartet, a Γ_7 doublet and a Γ_6 doublet with transverse ($E_\perp$) and longitudinal ($E_\parallel$) polarizations for specific orientations of the magnetic field. For $\vec{B}\parallel\langle 100\rangle$ and $\vec{B}\parallel\langle 111\rangle$, the selection rules with right circularly polarized radiation are given by the upper figure and those with left circularly polarized radiation by the lower figure.

	$\overline{T}_d$	$\vec{B}\parallel\langle 100\rangle$	$\vec{B}\parallel\langle 111\rangle$	$\vec{B}\parallel\langle 011\rangle$
$E_\perp$	Γ_8	$+1\quad -3$ $-1\quad +3$	$-1\quad +2$ $+1\quad -2$	0 ± 2
	Γ_7	$+1$ -1	$-1\quad +2$ $+1\quad -2$	0 ± 2
	Γ_6	-1 $+1$	$-1\quad +2$ $+1\quad -2$	± 1
$E_\parallel$	Γ_8	± 2	$0\quad \pm 3$	$\pm 1\quad \pm 3$
	Γ_7	± 2	0	± 1
	Γ_6	0	0	0 ± 2

impurity in silicon

$g_{3/2}(100) = 1.22$, $g_{1/2}(100) = 0.97$,

$g_1' = 0.93$, and $g_2' = 0.13$.

The expressions for g_1' and g_2' as functions of the valence-band parameters and of the amplitude of the wave functions are far from being simple, as can be seen from the expressions for $g_{3/2}(100)$ and $g_{1/2}(100)$ for germanium obtained for the Γ_8 s and p levels in Ref. 14. The same type of calculation has also been performed by Bir *et al.* for the acceptor ground state in silicon and germanium.[21]

III. EXPERIMENTAL TECHNIQUE

The monochromator used for the measurements is a Perkin-Elmer model 99G equipped with the appropriate gratings (20, 30, or 40 lines mm^{-1}). The radiation from the globar is reflected on a calcium- or barium-fluoride plate before entering the monochromator. Final filtering is accomplished through reflection on a gold-coated mirror (700 mesh) and the two polyethylene windows (each 1 mm thick) of the magneto-optical cryostat. The detector is a Perkin-Elmer thermopile with a CsI lens.[22] The radiation is polarized by a wire-grid polarizer on a polyethylene substrate.[23] Water vapor is removed by purging the whole system with dry nitrogen obtained by pressurizing a liquid-nitrogen tank. The maximum working resolution is limited by the aperture of the cryostat to ~0.09 meV and most spectra are taken with a resolution of 0.12 meV. Calibration of the monochromator is obtained by using selected water-vapor lines.[24,25] The reproducibility of the zero-field lines is ±0.01 meV.

The magnetic field is produced by a superconducting solenoid[26] made from niobium-titanium 25/33 wire, with a rated homogeneity of 0.1% in a spherical volume of 1 cm^3. The critical field is 71.4 kG, but the coil is never energized above a current of 24 A, corresponding to 64 kG. A sketch of the magneto-optical cryostat is given in Ref. 27. The components observed with $\vec{E} \parallel \vec{B}$ and $\vec{E} \perp \vec{B}$ are designated as the $E_\parallel$ and $E_\perp$ components, respectively. In order to observe the $E_\parallel$ components as a sample holder with two small gold-coated mirrors was designed and its effectiveness has been checked by observing the magnetoexcitation spectrum of phosphorus in silicon.[28]

The temperature of the sample is never less than 11 K (~1 meV). The over-all reproducibility of the position of the Zeeman components is approximately ±0.04 meV. An order of magnitude of the relative intensities of the Zeeman components is what can only be expected because of the size and the shape of the cryostat, which preclude the use of the "in" and "out" technique.

The samples were cut from float-zoned single-crystal ingots with net boron concentration $\lesssim 7\times10^{13}$ atoms/cm^3 and also from a pulled single-crystal ingot with 1.4×10^{14} (boron atoms)/cm^3. The best results were obtained with the samples cut from the float-zoned crystals. The samples were oriented with x rays and given an optical polish. At the end of the series of optical experiments, all the samples used were cross checked by taking Laue diagrams with them.

IV. EXPERIMENTAL RESULTS

The zero-field photoexcitation spectrum of boron impurity in silicon is shown in Fig. 1. The position of the lines is given in Table III; it is in good agreement with the values of Onton *et al.*[29] and of Chandrasekhar.[30]

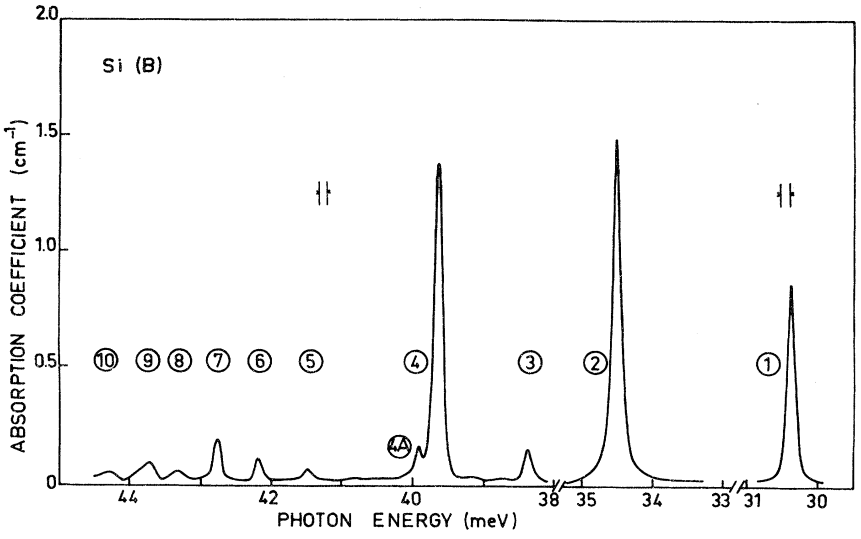

FIG. 1. Excitation spectrum of boron in float-zoned silicon. The net acceptor concentration is 7×10^{13} atoms/cm^3 for line 1 and 3×10^{13} atoms/cm^3 for the other lines.

TABLE III. Position (meV) of the absorption lines of boron impurity in silicon.

Line	Line position This work	Chandrasekhar[a]	Onton *et al.*[b]
1	30.37 ± 0.01	30.38	30.38
2	34.50 ± 0.02	34.52	34.53
3	38.38 ± 0.01	38.38	38.35
4	39.63 ± 0.02	39.63	39.64
4A	39.91 ± 0.02	39.92	39.91
5	41.47 ± 0.01		41.52
6	42.18 ± 0.01	42.18	42.19
7	42.75 ± 0.01	42.76	42.79
8	43.29 ± 0.03		43.27
9	43.74 ± 0.03		43.86
10	44.29 ± 0.02		
Raman line			22.7[c]

[a]Reference 30. The maximum error in position is estimated to be ± 0.01 meV.

[b]Reference 29. The maximum error in position is estimated to be 0.02 meV. In this reference, the position of line 6 was inadvertently given as 42.50 instead of 42.19 meV.

[c]Reference 16.

The Zeeman splitting of lines 1, 2, 3, 4, and 4A has been studied in the Faraday and in the Voigt configurations to obtain the $E_\perp$ and $E_\parallel$ components in the three characteristic orientations of the magnetic field. The $E_\parallel$ components of lines 2, 3, 4, and 4A were not recorded for $\vec{B} \parallel \langle 111 \rangle$. We have also compared some of the data obtained for $\vec{B} \parallel \langle 011 \rangle$ with those for $\vec{B} \parallel \langle 11\bar{2} \rangle$. The component of a line J ($J = 1$, 2, 3, and 4) are labeled A_J, B_J, etc., towards increasing energies. The position of the Zeeman components of lines 1 and 2 is extrapolated to zero field using a linear fit. This procedure seems to be justified as the intersections with the energy axis come very close to the energy of the line under study. An attempt to use the same least-squares fit for line 3 showed a small interaction between levels of line 3 and states of lower energy. For these three lines, however, $a(10^2\ \text{meV/kG}) = [E(B) - E_J]/B$ is plotted on the right-hand side of the figures giving the splitting as a function of the magnetic field as a

TABLE IV. Observed field dependence of the energies of the Zeeman components of lines 1 and 2 of boron in silicon for $\vec{B} \parallel \langle 100 \rangle$. Standard deviation ± 0.01 unless otherwise specified.

Component $E_\perp$	Component $E_\parallel$	a (10^2 meV/kG)	Component $E_\perp$	Component $E_\parallel$	a (10^2 meV/kG)
A_1		− 1.36	J_1		0.66
B_1		− 0.91 ± 0.02	K_1		1.24
	C_1	− 0.67			
D_1		− 0.57	A_2		− 1.43
	E_1	− 0.27		B_2	− 0.65
F_1		− 0.05		C_2	− 0.33
	G_1	0.12	D_2		− 0.03
H_1		0.35		E_2	0.79
	I_1	0.63	F_2		1.59 ± 0.02

TABLE V. Observed magnetic field dependence of the energies of the Zeeman components of line 3 of boron in silicon for $\vec{B} \parallel \langle 100 \rangle$. Linear and quadratic fit.

Component $E_\perp$	Component $E_\parallel$	a_{lin} (10^2 meV/kG)	a_{quad} (10^2 meV/kG)	b (10^4 meV/kG^2)
A_3		− 1.069 ± 0.016	− 0.803 ± 0.036	− 0.49 ± 0.07
	B_3	− 0.68		
C_3		− 0.612 ± 0.009	− 0.479 ± 0.054	− 0.24 ± 0.10
D_3		− 0.041 ± 0.003	− 0.089 ± 0.009	0.09 ± 0.02
	E_3	0.594 ± 0.012	0.435 ± 0.042	0.29 ± 0.08
F_3		0.726 ± 0.013	0.930 ± 0.046	− 0.37 ± 0.08
G_3		1.343 ± 0.012	1.506 ± 0.035	− 0.35 ± 0.07

direct check of the symmetry and magnitude of the splitting for the orientations studied. For the lines 4 and 4A, a least-squares fit of the type $E(B) = E_J + aB + bB^2$ was used for some components which proved amenable to this treatment.

General remarks can first be made regarding the splitting of the lines under study vs magnetic field. One important feature is the absence of apparent quadratic effect for the components of lines 1, 2, and 3 and another is their asymmetric splitting which is beyond experimental error. As in the case of the acceptors in germanium, some $E_\perp$ and $E_\parallel$ components are found to be nearly coincident, this being noteworthy in the splitting of line 2 for $\vec{B} \parallel \langle 110 \rangle$. The components of lines 4 and 4A exhibit an unambiguous quadratic shift but the least-squares fit cannot, however, be used for some components, either because of their mutual merging or because of the interaction between sublevels of the excited states. For these reasons no component could, for instance, be ascribed with certainty to line 4A when $\vec{B} \parallel \langle 100 \rangle$. From Tables IV–XII, which give the splitting parameters of the various Zeeman components under different orientations of the magnetic field, it is found that the ratio of the maximum over minimum splitting with respect to the magnetic field orientation, $\Delta a_{\max}/\Delta a_{\min}$ (Δa is the difference between the components with the greatest positive and negative splitting parameters), is very similar for lines 1 and 3: $\Delta a_{100}/\Delta a_{111} = 1.34$ for line 1 and $\Delta a_{110}/\Delta a_{111} = 1.33$ for line 3. For line 2, $\Delta a_{110}/\Delta a_{111} = 1.04$, which reflects the very small dependence of the extreme components of this line on magnetic field orientation. The result for the linear parameters of line 4 is $\Delta a_{111}/\Delta a_{110} = 1.18$. It can be seen that the greatest energy difference between the extreme components is observed for line 4 when $\vec{B} \parallel \langle 111 \rangle$; it is given by $\Delta E_{\max}(\text{meV}) = 3.47 \times 10^{-2} B(\text{kG}) + 0.17 \times 10^{-4} B^2(\text{kG}^2)$. By comparison, for line D of boron in germanium, the maximum splitting at low fields is $\Delta E_{100}(\text{meV}) = 3.61 \times 10^{-2} B(\text{kG}) - 3.19 \times 10^{-4} B^2(\text{kG}^2)$, whereas at high fields, $\Delta E_{111}(\text{meV}) = 2.32 \times 10^{-2} B(\text{kG}) + 2.43 \times 10^{-4} B^2(\text{kG}^2)$, which emphasizes the im-

TABLE VI. Observed magnetic field dependence of the energies of some of the Zeeman components of line 4 of boron in silicon for $\vec{B} \parallel \langle 100 \rangle$. The position of the other components (lines 4 and 4A) is given for a field magnitude of 64 kG with a maximum error of ±0.02 meV.

Component $E_\perp$	Component $E_\parallel$	a (10^2 meV/kG)	b (10^4 meV/kG^2)	Component $E_\perp$	Component $E_\parallel$	Position (meV)
	A_4	−1.340 ± 0.028	0.97 ± 0.05	E_4		39.82
B_4		−0.851 ± 0.031	0.36 ± 0.06	F_4		40.08
C_4		−0.699 ± 0.035	1.01 ± 0.07		G_4[a]	40.30
	D_4	−0.306 ± 0.024	0.50 ± 0.05	K_4[a]		41.08
H_4		0.753 ± 0.025	0.78 ± 0.04	L_4[a]		41.27
I_4		1.019 ± 0.084	0.82 ± 0.15			
	J_4	1.890 ± 0.058	0.47 ± 0.11			

[a]Belongs to the line 4A.

portance of the quadratic effect in germanium.[12] In silicon, the quadratic effect is less than for boron and thallium in germanium; it is always positive for lines 4 and 4A but the two signs are equally found for line 3. From what has been said it is the quadratic effect of the excited sublevels, since no quadratic effect has been detected for the lines 1 and 2.

A. $\vec{B} \parallel \langle 100 \rangle$

The splittings observed at high field for the lines studied are shown in Figs. 2 and 3, and the magnetic field dependence of the components in Figs. 4 and 5. Tables IV–VI give the experimental splitting parameters. Line 1 splits into seven and four components for $E_\perp$ and $E_\parallel$, respectively. The width of the $E_\perp$ components is resolution-limited to 0.12 meV with the sample used ($N_a - N_d = 7 \times 10^{13}$ cm^{-3}) but the $E_\parallel$ components recorded with the Czochralski-grown sample with $N_a - N_d = 1.4 \times 10^{14}$ cm^{-3} are broader. The $E_\parallel$ spectrum of line 1 shows a low-energy thermalization effect, the actual intensity of component I_1 being, however, less than that shown because of a residual water-vapor line. The splitting of line 2 for $E_\perp$ is very simple, but the components are broader than those of line 1. A $E_\perp$ spectrum recorded in the Voigt configuration ($\vec{k} \parallel \langle 001 \rangle$) shows a higher contrast than that recorded in the Faraday configuration (Fig. 2). The $E_\parallel$ spectrum of line 2 is very broad and it is asymmetric. The $E_\perp$ Zeeman pattern for line 3 consists in five well-defined components; it is shown in Fig. 3 for a field of 40 kG since for higher values of the field, component G_3 and component A_4 get mixed. The $E_\parallel$ spectrum shows a broad low-energy band which may be due to unresolved components and a well-resolved high-energy component. It is noteworthy that in both spectra, the low-energy components are more intense than the high-energy one, indicating a depopulation of the ground-state sublevels associated to the high-energy components and/or an asymmetry in the strength of the transitions due to the proximity of lines 4 and 4A. (It is seen, however, that component G_3 does not experience a strong repulsion from the components of line 4.) In the case of lines 4 and 4A, eight components are observed when $\vec{E} \perp \vec{B}$ using a resolution of 0.09 meV, and four when $\vec{E} \parallel \vec{B}$. A ninth $E_\perp$ component is observed for values of the magnetic field between 28 and 48 kG. It belongs probably to 4A, but it merges with the I_4 component at high fields and it is not tabulated. On the other hand, the component E_4 is observed only at 60 and 64 kG and its assignment to either lines 4 or 4A is not clear cut, its assignment to line 5 being, however, problematic. The component G_4 behaves as if belonging to line 4A, but it is relatively strong and this means a strong interaction with line 4. The components K_4 and L_4 belong very probably to line 4A, but we have not calculated the splitting parameters for these components as we ignore the possible interactions between the sublevels of lines 4 and 4A.

B. $\vec{B} \parallel \langle 011 \rangle$ and $\vec{B} \parallel \langle 211 \rangle$

The results pertinent to $\vec{B} \parallel \langle 011 \rangle$ are given in Figs. 6–9 and in Tables VII–IX. The $E_\parallel$ spectra

TABLE VII. Observed magnetic field dependence of the energies of the Zeeman components of lines 1 and 2 of boron in silicon for $\vec{B} \parallel \langle 011 \rangle$. Standard deviation ±0.01 unless otherwise specified.

Component $E_\perp$	Component $E_\parallel$	a (10^2 meV/kG)	Component $E_\perp$	Component $E_\parallel$	a (10^2 meV/kG)
A_1		−0.92	C_2		−0.76
B_1		−0.64		D_2	−0.72
	C_1	−0.45	E_2		−0.06
D_1		−0.30		F_2	−0.03
	E_1	0.33		G_2	0.54 ± 0.03
F_1		0.34	H_2		0.59
G_1		0.64	I_2		0.85
	H_1	0.93		J_2	0.90
I_1		1.56		K_2	1.51
			L_2		1.62
	A_2	−1.45			
B_2		−1.40			

TABLE VIII. Observed magnetic field dependence of the energies of the Zeeman components of line 3 of boron in silicon for $\vec{B} \parallel \langle 011 \rangle$. Linear and quadratic fit.

Component $E_\perp$	Component $E_\parallel$	a_{lin} (10^2 meV/kG)	a_{quad} (10^2 meV/kG)	b (10^4 meV/kG^2)
A_3		-0.948 ± 0.008	-1.070 ± 0.031	0.22 ± 0.06
	B_3	-0.255 ± 0.006	-0.149 ± 0.026	-0.19 ± 0.05
C_3		-0.179 ± 0.011	0.016 ± 0.021	-0.35 ± 0.04
D_3		0.244 ± 0.005	0.214 ± 0.041	0.05 ± 0.07
	E_3	0.467 ± 0.016	0.215 ± 0.047	0.46 ± 0.09
	F_3	1.012 ± 0.015	0.787 ± 0.051	0.41 ± 0.09
G_3		1.68		

were recorded with $\vec{k} \parallel \langle 111 \rangle$. A low-intensity high-energy component is observed in both configurations for line 1. The shoulder on the low-energy side of E_1 corresponds probably to an unresolved component. The near coincidence between the $E_\parallel$ and $E_\perp$ splittings of line 2 has already been mentioned; this phenomenon is also observed in the splitting of line D of boron in germanium for the three orientations studied. The $E_\perp$ component observed at 60 and 64 kG between components B_4 and E_4 has been attributed to line 3 and consequently labeled G_3 despite the fact that it is not seen at low fields, but, generally speaking, interpretation of data of line 3 is made sometimes difficult owing to the small intensity of this line. Component L_4 belongs to line 4A; the behavior of component J_4 of line 4 can be qualitatively explained by an interaction with an upper sublevel. For $\vec{B} \parallel \vec{E} \parallel \langle 011 \rangle$, two lines were observed for values of the magnetic field greater or equal to 60 kG on the high-energy side of the spectrum, but they could not be correlated to components of either line 4A or line 4.

Figure 6 shows the splitting of line 2 when $\vec{B} \parallel \langle 211 \rangle$. The superposition of the $E_\perp$ components of this line when $\vec{B} \parallel \langle 110 \rangle$ and $\vec{B} \parallel \langle 211 \rangle$ is shown in Fig. 10 and this situation is predicted theoretically. Similar results are obtained for line 1 in both configurations. This is not the case for the group of lines 4 and 4A, as can be seen by comparison of Tables IX and X, and also for line 3, which is additional evidence for the existence of interactions of sublevels of this group among themselves or with upper ones.

C. $\vec{B} \parallel \langle 111 \rangle$

The data for this orientation of the magnetic field are reported last because lines 2, 3, 4, and 4A were not studied for $\vec{E} \parallel \vec{B}$. They are presented in Figs. 11–14 and in Tables X and XII. The number of components of line 1 is smaller in comparison with that for the other orientations, indicating a superposition of the transitions. The same low-energy thermalization effect as for $\vec{B} \parallel \langle 100 \rangle$ is observed in the $E_\perp$ spectrum but the $E_\parallel$ spectrum bears a strong similarity with that for $\vec{B} \parallel \langle 110 \rangle$. The extreme components of line 2 exhibit the same splitting as for $\vec{B} \parallel \langle 100 \rangle$ and $\vec{B} \parallel \langle 110 \rangle$ and the pattern is very similar to that observed for $\vec{E} \perp \vec{B} \parallel \langle 110 \rangle$. The width of the components of lines 3, 4, and 4A is resolution limited to ~0.10 meV. The components E_4 and H_4 can be attributed to line 4A. The observed splitting of line 3 is very asymmetric, but it is surprising to note in Table XI the correlation between the splitting parameters for that line and those for the low-energy components of line 2 for that orientation of the magnetic field. It can be fortuitous but it can also indicate a resemblance between the two excited levels responsible for these two lines, which can manifest itself only when interaction with other levels is negligible.

V. DISCUSSION

It has been theoretically established that the ground state of the acceptor levels is a Γ_8 state and that the excited states can be Γ_8, Γ_7, and Γ_6 states or a combination of them. The results obtained by piezospectroscopy [8,29] imply that the excited levels of lines 1, 2, and 3 have Γ_8 symmetry whereas the data for the lines 4 and 4A can be interpreted by assuming that the excited levels have $\Gamma_6 + \Gamma_7$ and Γ_8 symmetry, respectively.

TABLE IX. Observed magnetic field dependence of the energies of some of the Zeeman components of lines 4 and 4A of boron in silicon for $\vec{B} \parallel \langle 011 \rangle$. The position of the other components is given for a field magnitude of 64 kG with a maximum error of ±0.02 meV.

Component $E_\perp$	Component $E_\parallel$	a (10^2 meV/kG)	b (10^4 meV/kG^2)	Component $E_\perp$	Component $E_\parallel$	Position (meV)
A_4		-1.359 ± 0.031	0.57 ± 0.06		C_4	39.43
B_4		-0.962 ± 0.115	0.35 ± 0.20	E_4		39.84
	D_4	-0.653 ± 0.039	0.90 ± 0.07	F_4		39.98
	H_4	0.771 ± 0.033	0.25 ± 0.06	G_4		40.16
	I_4	0.886 ± 0.084	1.05 ± 0.15	J_4[a]		40.66
K_4		1.570 ± 0.061	1.07 ± 0.11			
L_4[a]		1.753 ± 0.044	0.30 ± 0.10			

[a]Belongs to line 4A.

TABLE X. Observed magnetic field dependence of the energies of the $E_\perp$ Zeeman components of lines 4 and 4A of boron in silicon for $\vec{B} \parallel \langle 211 \rangle$. For the component E_4 the position (meV) is given at 64 kG.

Component	a (10^2 meV/kG)	b (10^4 meV/kG^2)
A_4	-1.436 ± 0.018	0.98 ± 0.03
B_4	-0.684 ± 0.027	0.86 ± 0.05
C_4	0.194 ± 0.028	0.42 ± 0.05
D_4	0.539 ± 0.059	1.01 ± 0.11
F_4[a]	1.790 ± 0.010	0.38 ± 0.02
E_4	40.85	

[a]Belongs to line 4A.

The spin-resonance experiments of Feher *et al.*[15] yielding $g_{1/2} = g_{3/2} = 1.21$ for the ground state of the boron acceptor in silicon under uniaxial stress are in agreement with the ordering deduced from the calculation of Suzuki *et al.*[13] A consequence of the equality between the values of $g_{1/2}$ and $g_{3/2}$ is the isotropy of the splitting of the ground state with $g_1' = 1.21 \pm 0.01$ and $r = 0$. The magneto-Raman experiments of Cherlow *et al.* provided the self-consistent spectroscopic values $g_1' = 0.84 \pm 0.09$, $g_2' = 0.13 \pm 0.08$, and, $r = 0.15 \pm 0.11$, which accounted for the small anisotropy observed.[16] No calculation has been performed for the excited states and we must try to find a method to reach the ordering of the levels and their g factors. Moreover, we have no experimental evidence of the symmetry of the splitting of the ground state under a magnetic field, i.e., of the coincidence of the centers of gravity of the states with $m_j = \pm \frac{1}{2}$ and $m_j = \pm \frac{3}{2}$. At zero field, the random internal strains broaden the states with Γ_8 symmetry. This broadening is thought to prevent the observation of the paramagnetic resonance of the bound holes in silicon, as it leads to a very short spin-lattice relaxation time. When a magnetic field is applied, the stress-induced broadening can also produce an asymmetry in the splitting of the state. Our results and measurements by Chandrasekhar[30] show that most boron absorption lines have an observed width of approximately 0.08 meV at concentrations where impurity broadening is negligible. Then, an upper limit of 0.06 and 0.02 meV for the widths of the ground and excited states, respectively, is not an unreasonable figure. We have, however, no direct experimental evidence of a splitting of the ground state greater than 0.03 meV and we subsequently assume a symmetric splitting of this state under a magnetic field.

A. Line 1

Using as a starting point the g values obtained by Cherlow *et al.*, we first considered line 1; for this line, identified as a $\Gamma_8 \rightarrow \Gamma_8$ transition,[8] 12 components are predicted when $\vec{B} \parallel \langle 100 \rangle$ and 11 are actually observed. The relative intensities and the positions of the four expected $E_\parallel$ components gave a first scheme which yielded the position of the Faraday components with a reasonable accuracy. The assignment of the observed components to specific transitions is given in Fig. 15. It is found that the observed splitting can account for the 12 allowed transitions if we assume component F_1 to be due to the superposition of two transitions, namely, $\frac{1}{2} \rightarrow -\frac{1}{2}$ and $-\frac{1}{2} \rightarrow \frac{1}{2}$. One major point is that in order to obtain a self-consistent fit, we are faced with an asymmetric splitting of the excited state with $g_{3/2}^{(1)}(100) < g_{1/2}^{(1)}(100) < 0$. The centers of gravity of both the $m_j = \pm \frac{1}{2}$ and $m_j = \pm \frac{3}{2}$ sublevels are shifted downwards with respect to the zero-field position of line 1, under the assumption of a symmetric splitting of the ground state.

TABLE XI. Observed magnetic field dependence of the energies of the Zeeman components of lines 1, 2, and 3 of boron in silicon for $\vec{B} \parallel \langle 111 \rangle$. For lines 2 and 3, only the $E_\parallel$ components are listed. For the line 3, a_{quad} is not given in the table.

Component		a	Component	a_{lin}	b
$E_\perp$	$E_\parallel$	(10^2 meV/kG)	$E_\perp$	(10^2 meV/kG)	(10^4 meV/kG^2)
A_1		-1.02	E_2	0.94	
	B_1	-0.42	F_2	1.55	
C_1		-0.33			
D_1		0.14	A_3	-1.42	-0.17 ± 0.12
	E_1	0.34	B_3	-0.71	-0.19 ± 0.05
F_1		0.92	C_3	0.07	0.17 ± 0.08
			D_3	0.58	0.06 ± 0.16
A_2		-1.41			
B_2		-0.75			
C_2		0.0			
D_2		0.58			

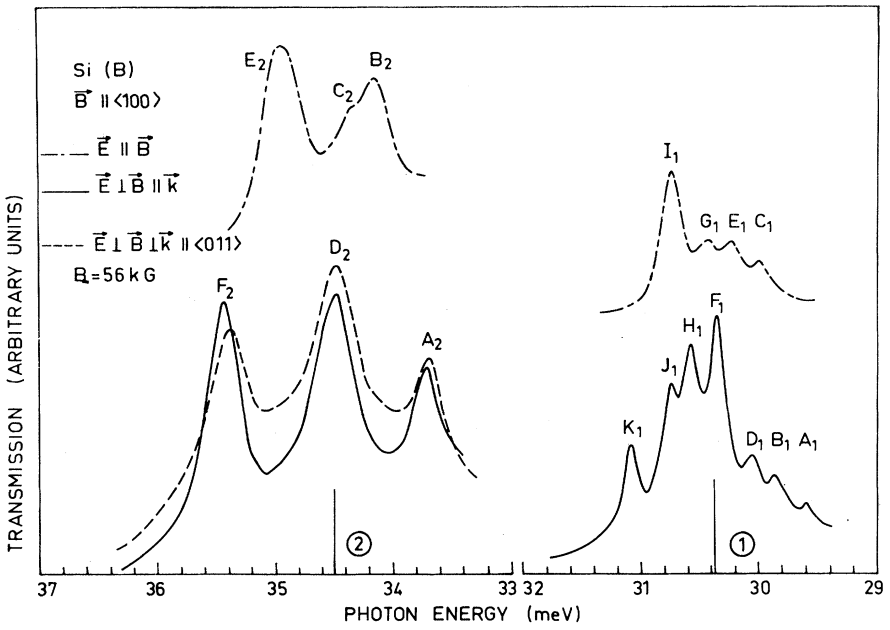

FIG. 2. Zeeman splitting of lines 1 and 2 of boron in silicon for $\vec{B} \parallel \langle 100 \rangle$. The origins have been displaced for the sake of clarity.

This is the reason why we have defined two additional parameters $s_{\pm 1/2}(1)$ and $s_{\pm 3/2}(1)$ to describe the splitting of the line:

$$s_{\pm m_j}(J) = \{[E_{Jm_j}(B) + E_{J-m_j}(B)]/2 - E_J\}/B \,,$$

where E_{Jm_j} is the position of the m_j excited sublevel of line J.

For the ground state, we obtain an average value of 1.12 ± 0.02 for $g_{3/2}(100)$, in good agreement with the value of 1.13 ± 0.03 given by Cherlow *et al.* Now, for each $\Gamma_8 \rightarrow \Gamma_8$ transition studied, we hope to find, for $\vec{B} \parallel \langle 100 \rangle$ two spacings which give directly $g_{1/2}(100)$, that is $[-\frac{1}{2} \rightarrow \frac{3}{2}] - [\frac{1}{2} \rightarrow \frac{3}{2}]$ and $[-\frac{1}{2} \rightarrow -\frac{3}{2}] - [\frac{1}{2} \rightarrow -\frac{3}{2}]$. If we use $g_{1/2}(100) = 0.88 \pm 0.06$ derived in Ref. 16, we expect to find a spacing of ~ 0.33 meV between some $E_\parallel$ and $E_\perp$ components at 64 kG, and we observe in fact an energy difference of 0.35 meV between components J_1 and G_1; with the same value for $g_{1/2}(100)$, we must also obtain four times an energy difference of ~ 0.79 meV at 64 kG between $E_\perp$ components corresponding to the spacing between the ground-state sublevels with $\Delta m_j = \pm 2$, always under the assumption of a symmetric splitting of the ground state. All the energy differences found experimentally yielded an average value of 0.82 meV. The difference is small by itself, but the fact is that it systematically favors a higher value for $g_{1/2}(100)$. By taking also into consideration the splitting of lines 3 and 4 for $\vec{B} \parallel \langle 100 \rangle$, we have adopted an average value $g_{1/2}(100) = 1.04 \pm 0.06$.

TABLE XII. Observed magnetic field dependence of the energies of the $E_\perp$ Zeeman components of lines 4 and 4A of boron in silicon for $\vec{B} \parallel \langle 111 \rangle$.

Component	a (10^2 meV/kG)	b (10^4 meV/kG^2)
A_4	-1.764 ± 0.021	0.14 ± 0.04
B_4	-1.399 ± 0.033	1.15 ± 0.06
C_4	-0.611 ± 0.035	0.96 ± 0.07
D_4	0.246 ± 0.015	0.10 ± 0.03
E_4 [a,b]	0.11	
F_4	0.641 ± 0.054	1.04 ± 0.10
G_4	1.711 ± 0.034	0.31 ± 0.06
H_4 [a]	1.733 ± 0.034	0.64 ± 0.07

[a]Belongs to line 4A. [b]Linear fit.

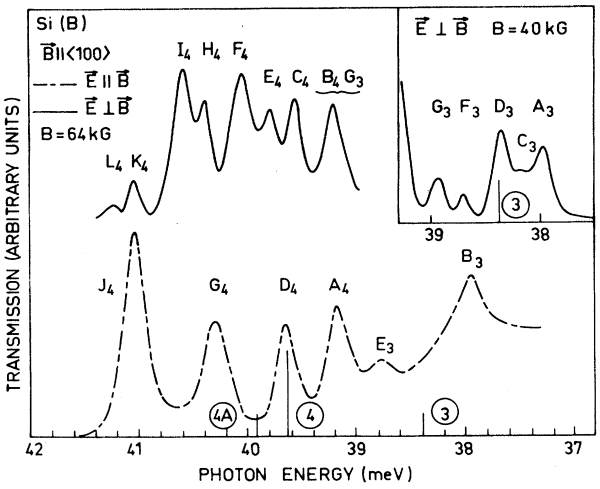

FIG. 3. Zeeman splitting of lines 3, 4, and 4A of boron in silicon for $\vec{B} \parallel \langle 100 \rangle$. The origins have been displaced.

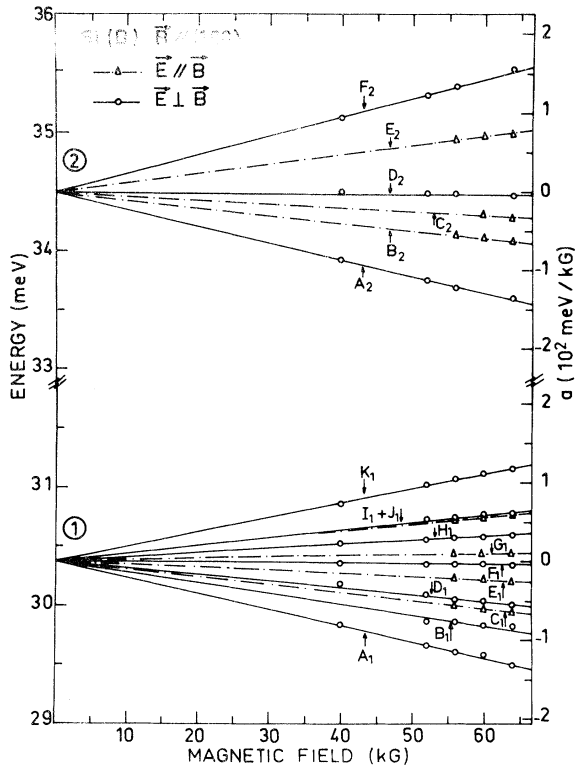

FIG. 4. Magnetic field dependence of the splitting of lines 1 and 2 for $\vec{B} \parallel \langle 100 \rangle$. The scale on the right-hand side gives the splitting parameters of the components.

This value minimizes the anisotropy of the splitting of the ground state, by comparison with that obtained by the magneto-Raman scattering experiments, but it remains, however, substantially lower than the value obtained by spin resonance. The comparison of the experimental g factors of the ground state of boron in silicon with theoretical results are shown in Table XIII. The agreement with the values of Suzuki *et al.* can be considered as acceptable considering the uncertainty in the experimental results and that the theoretical results are independent of the atomic number of the impurity. It is felt that experiments at temperature of ~20 K with higher resolution could improve the accuracy on the values of $g_{1/2}(100)$ and $g_{3/2}(100)$.

The g factors for the excited state of line 1 are both negative with $g^{(1)}_{3/2}(100) = -0.57 \pm 0.04$ and $g^{(1)}_{1/2}(100) = -1.09 \pm 0.05$, and this allows for a marked anisotropy of the splitting of this state, with $g'_1(1) = -1.16 \pm 0.06$ and $r_1 = -0.05 \pm 0.08$, which is not too far from the idealized value $-\frac{1}{13} = -0.079$.

As already mentioned, a quantitative comparison of the intensities of the observed components in order to compare them with theory is difficult because we recorded only the transmission spectrum and also because of the thermalization of the population of the ground-state sublevels, but this is, however, necessary to decide whether we can observe or not a given transition for the other orientations of the magnetic field. If we consider Fig. 15, we see that the components K_1 and H_1 both arise from the $-\frac{3}{2}$ ground-state sublevel. Their relative intensities should be $I_{K_1}/I_{H_1} = -1 + 4(1+v_1)/3u_1$ by using the appropriate relations of Ref. 20. Experimentally I_{K_1}/I_{H_1} is between 0.6 and 0.8. If we take 0.7 for this ratio, we have $4(1+v_1)/3u_1 = 1.7$. The inspection of the $E_{\parallel}$ spectrum of line 1 shows that v_1 must be small, and as we only need an order of magnitude, we put $v_1 = 0$, hence $u_1 = 0.8$. We have then obtained for the Zeeman components of line 1 the relative intensities of Table XIV. No estimation of the uncertainty was actually made. For $\vec{B} \parallel \langle 111 \rangle$, the splitting observed for line 1 is very simple. This simplicity can be explained if we assume that $g_{1/2}(111)$ is small compared to what is observed for $\vec{B} \parallel \langle 100 \rangle$. An independent analysis produced the level scheme of Fig. 16. The $E_{\parallel}$ transitions $\pm\frac{3}{2} \rightarrow \mp\frac{3}{2}$ are not observed and this is not inconsistent with the relative intensities predicted from the values of u_1, v_1, and r_1 obtained from $\vec{B} \parallel \langle 100 \rangle$ and shown in Table XV. The strong E_1 component is ascribed to the superposition of the $-\frac{3}{2} \rightarrow -\frac{3}{2}$ and $-\frac{1}{2} \rightarrow -\frac{1}{2}$ transitions plus a small residual water-vapor line. The B_1 component corresponds to the same type of transition, i.e., $\frac{3}{2} \rightarrow \frac{3}{2}$ and $\frac{1}{2} \rightarrow \frac{1}{2}$, the difference with E_1 being due to the thermalization of the sublevels of the

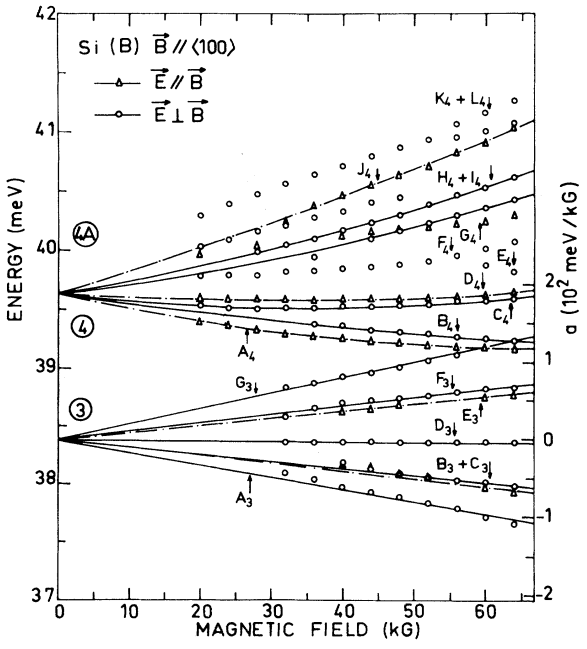

FIG. 5. Magnetic field dependence of the splitting of lines 3, 4, and 4A for $\vec{B} \parallel \langle 100 \rangle$.

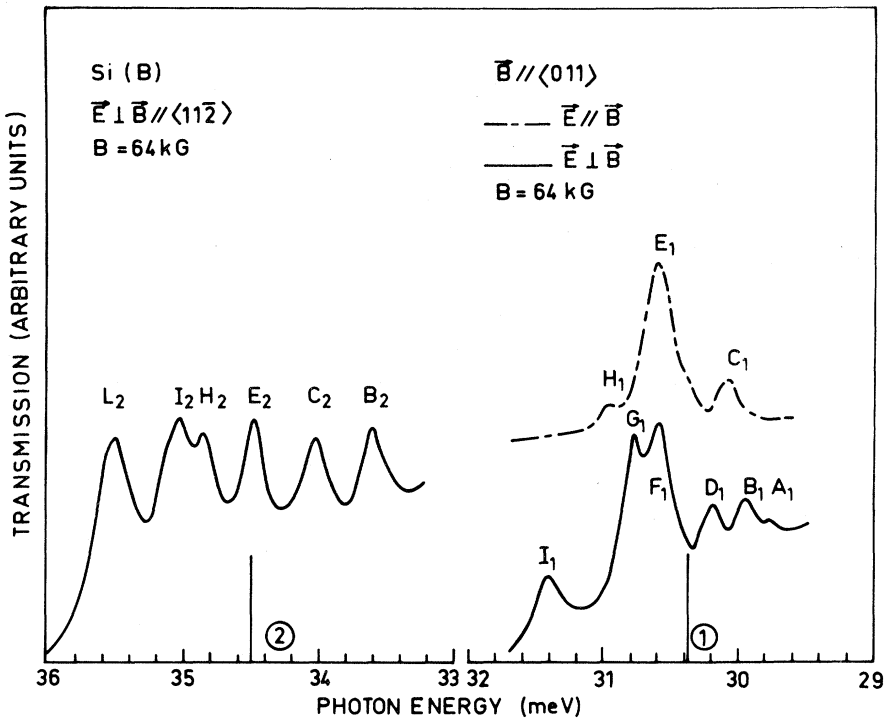

FIG. 6. Zeeman splitting of line 1 of boron in silicon for $\vec{B} \parallel \langle 011 \rangle$ and line 2 for $\vec{E} \perp \vec{B} \parallel \langle 11\bar{2} \rangle$. For line 1, the origins are displaced.

ground state. The predicted intensities of the $-\frac{3}{2} \rightarrow \frac{3}{2}$ and $\frac{3}{2} \rightarrow -\frac{3}{2}$ transitions are much weaker and we think that this is the reason why they are not observed. In the $E_\perp$ case, the component F_1 is ascribed to the superposition of three transitions, $-\frac{3}{2} \rightarrow -\frac{1}{2}$ and $-\frac{3}{2} \rightarrow \frac{1}{2}$, separated by ~0.10 meV at 64 kG, and $-\frac{1}{2} \rightarrow \frac{3}{2}$. The component A_1 is ascribed to the corresponding transitions $\frac{3}{2} \rightarrow -\frac{1}{2}$, $\frac{3}{2} \rightarrow \frac{1}{2}$ and to $\frac{1}{2} \rightarrow -\frac{3}{2}$, its intensity being reduced by thermalization. The splitting of the excited states and the ordering of the sublevels are consistent with what is derived from the results for $\vec{B} \parallel \langle 100 \rangle$. We derive directly a splitting of 0.10 meV at 64 kG for the $\pm\frac{1}{2}$ sublevels while we obtain from $g_1'^{(1)}$ and $r_1 g_{1/2}^{(1)}(111) = -0.31$, corresponding to a splitting of 0.12 meV at the same field, which is not too unsatisfactory considering the accuracy of the results.

It should be noted that, when considering the selection rules alone, there is a double degeneracy regarding the sign of $g_{3/2}(111)$ since the level scheme of Fig. 16 satisfies also the selection rules if the $m_j = \frac{3}{2}$ and $m_j = -\frac{3}{2}$ sublevels are inverted, as they both correspond to the same irreducible representation of point group $\bar{C}_3$.

The situation for $\vec{B} \parallel \langle 011 \rangle$ has been analyzed independent of the experimental data for that orientation and the proposed level scheme is given in Fig. 17. Exclusive of the magnitude of the shift of the excited sublevels, the results are consistent with those obtained for $\vec{B} \parallel \langle 100 \rangle$.

The absence of the component associated with the $\frac{3}{2} \rightarrow -\frac{1}{2}$ transition is very likely due to thermalization, considering the intensity of I_1; the broad

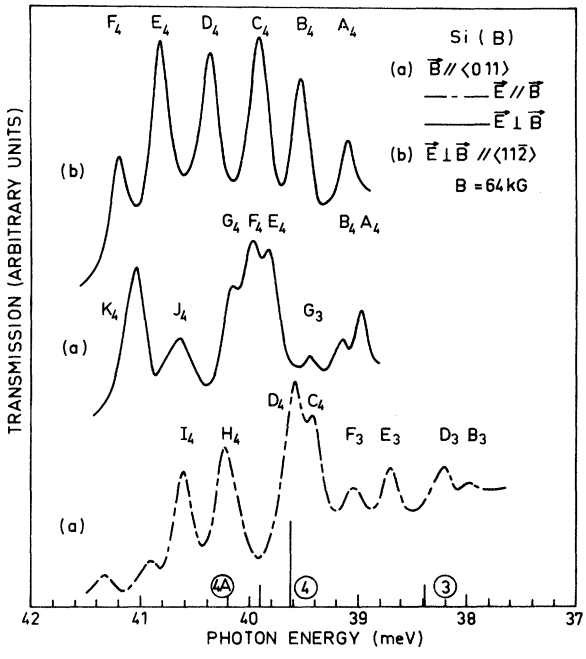

FIG. 7. Zeeman splitting of lines 3, 4, and 4A of boron in silicon for $\vec{B} \parallel \langle 011 \rangle$ and for $\vec{E} \perp \vec{B} \parallel \langle 11\bar{2} \rangle$. The origins have been displaced.

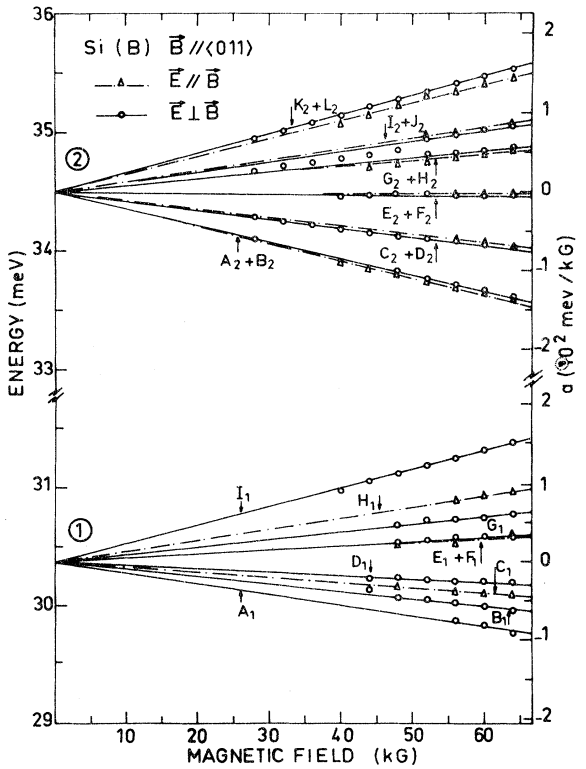

FIG. 8. Same as Fig. 4 for $\vec{B} \| \langle 011 \rangle$.

component F_1 is ascribed to the superposition of the $-\frac{1}{2} \rightarrow \frac{3}{2}$ and $\frac{1}{2} \rightarrow \frac{1}{2}$ transitions, having energy differences of 0.07 meV at 64 kG. The weakness

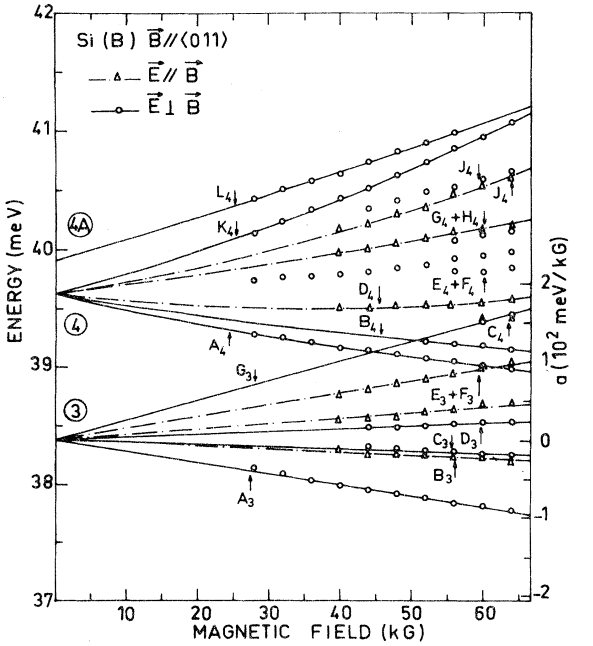

FIG. 9. Same as Fig. 5 for $\vec{B} \| \langle 011 \rangle$.

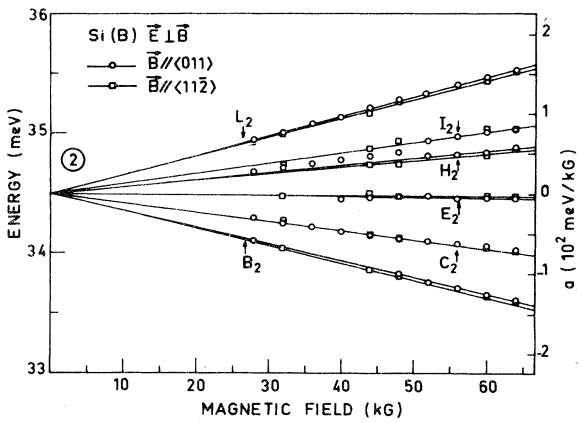

FIG. 10. Comparison of the magnetic field dependence of the splitting of line 2 when $\vec{B} \| \langle 011 \rangle$ and $\vec{B} \| \langle 11\bar{2} \rangle$

of the H_1 component, attributed to the superposition of the $-\frac{3}{2} \rightarrow \frac{3}{2}$ and $-\frac{1}{2} \rightarrow \frac{1}{2}$ transitions can explain why the $\frac{3}{2} \rightarrow -\frac{3}{2}$ and $\frac{1}{2} \rightarrow -\frac{1}{2}$ transitions go unobserved. The shoulder on the low-energy side of the component E_1 can be quite plausibly ascribed to the $-\frac{1}{2} \rightarrow -\frac{3}{2}$ transition, whereas line C_1 is attributed to the superposition of the $\frac{1}{2} \rightarrow \frac{3}{2}$ and $\frac{3}{2} \rightarrow \frac{1}{2}$ transitions. In Table XVI are listed the splitting parameters of the allowed transitions associated with line 1 for $\vec{B} \| \langle 011 \rangle$ deduced from the empirical level scheme of Fig. 17. We have also included in this table the relative intensities of the transitions obtained by using the relations given in Ref. 20 for $\vec{B} \| [110]$, $\vec{E} \| [\bar{1}10]$. This condition of polarization is not fulfilled in our experiments as the incident beam is predominantly polarized parallel to [111], but there seems to be, however, a gross correlation with what is observed for the $E_\perp$ components, specially for the relative intensity of I_1. For the $E_\parallel$ components, the relative intensities of E_1 and of (H_1, H_1') are in qualitative agreement with the observed spectrum of Fig. 6.

The downwards shift of the centers of gravity of the excited sublevels is again more pronounced for the $\pm\frac{3}{2}$ sublevels than for the $\pm\frac{1}{2}$ sublevels, the latter being roughly at the same position as that of the zero-field levels while the former experience a shift of $\sim -1.4 \times 10^{-3}$ meV/kG. The results obtained for line 1 are summarized in Table XVII.

B. Line 2

The behavior of line 2, assumed to be due to a $\Gamma_8 \rightarrow \Gamma_8$ transition, has been interpreted on the basis of the results for $\vec{B} \| \langle 011 \rangle$. The near coincidence of the highest- and lowest-energy components for the three orientations of the magnetic field together with the similarity of the $E_\parallel$ and $E_\perp$ spectra for $\vec{B}_\parallel \langle 011 \rangle$ was explained by reference to Table I: It

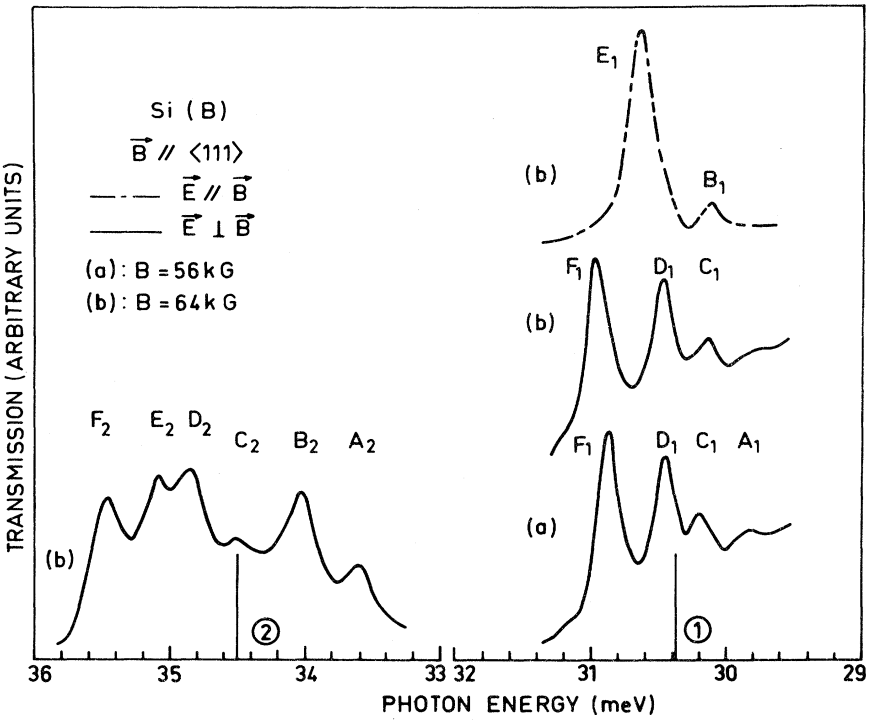

FIG. 11. Same as Fig. 2 for $\vec{B} \parallel \langle 111 \rangle$. Note the thermalization of the component A_1 at 64 kG.

is seen there that for the "forbidden" value $r = -\frac{1}{7}$, a Γ_8 level splits into an isotropic doublet and this could qualitatively explain the splitting observed.

For $\vec{B} \parallel \langle 011 \rangle$, we obtained the level scheme of Fig. 18 and from this, we derived a self-consistent fit which produced $g^{(2)}_{1/2}(110) = 1.79 \pm 0.12$ and $g^{(2)}_{3/2}(110) = 0.54 \pm 0.04$. This allows the calculation of $g'_1(2)$ and of r_2. We found $g'_1(2) = -2.17 \pm 0.76$ and $r_2 = -0.137 \pm 0.08$, very near the idealized case $r = -\frac{1}{7} = -0.143$. The quantitative assignment of the components observed for $\vec{B} \parallel \langle 011 \rangle$ is given in Table XVIII using the above g factors. It was not possible to distinguish reliably between the respective positions of the $-\frac{1}{2}$ and $-\frac{3}{2}$ excited sublevels, but the difference for the $\frac{1}{2}$ and $\frac{3}{2}$ sublevels is thought to be significant. The splitting for $\vec{B} \parallel \langle 111 \rangle$ can be deduced from the above discussion and the result is shown in Fig. 19 and in Table XIX. The component C_2^+ has the same position and about the expected intensity of a residual-water-vapor line, but we have no reason to discard it as it fits correctly the proposed level scheme. Little can be said on the relative intensities of the components. The agreement between what is observed and the transition energy when $\vec{B} \parallel \langle 100 \rangle$ is only fair (Table XX) and the result given in Fig. 20.

We must assume the strong line D_2 to be due to the superposition of the $-\frac{1}{2} \rightarrow \frac{1}{2}$, $-\frac{1}{2} \rightarrow -\frac{3}{2}$, $\frac{1}{2} \rightarrow \frac{3}{2}$, and $\frac{1}{2} \rightarrow -\frac{1}{2}$ transitions. The assumption of the combination of $\Gamma_8 \rightarrow \Gamma_6$ and $\Gamma_8 \rightarrow \Gamma_7$ transitions to describe the behavior of line 2 under a magnetic field is not realistic: if this allows, on one hand, for the apparent isotropy of the splitting, it implies, on the other hand, $g_6(2) \simeq g_7(2) \simeq -1.7$ to

TABLE XIII. Comparison of the experimental g factors for the ground state of boron in silicon with theoretical estimations.

	This work	Cherlow *et al.*[a]	Feher *et al.*[b]	Suzuki *et al.*[c]	Bir and Butikov[d]
$g_{1/2}(100)$	1.04 ± 0.06	0.88 ± 0.06	1.21 ± 0.01	0.97	0.75
$g_{3/2}(100)$	1.12 ± 0.02	1.13 ± 0.03		1.22	0.72
g'_1 or K	1.03 ± 0.07	0.84 ± 0.09	1.21 ± 0.01	0.93	0.76
g'_2 or L	0.04 ± 0.04	0.13 ± 0.08	0.00 ± 0.01	0.13	-0.02

[a]Reference 16.
[b]Reference 15.
[c]Reference 13.
[d]Reference 21.

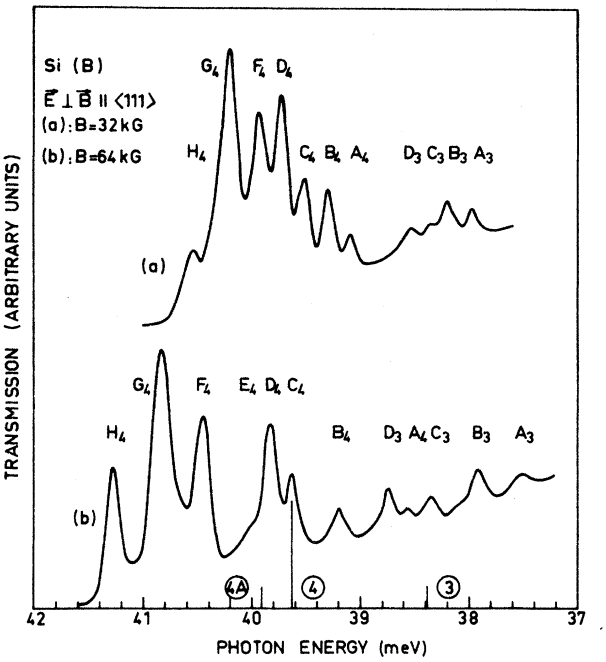

FIG. 12. Same as Fig. 3 for $\vec{B} \parallel \langle 111 \rangle$. Note the increase in intensity of component H_4 at 64 kG.

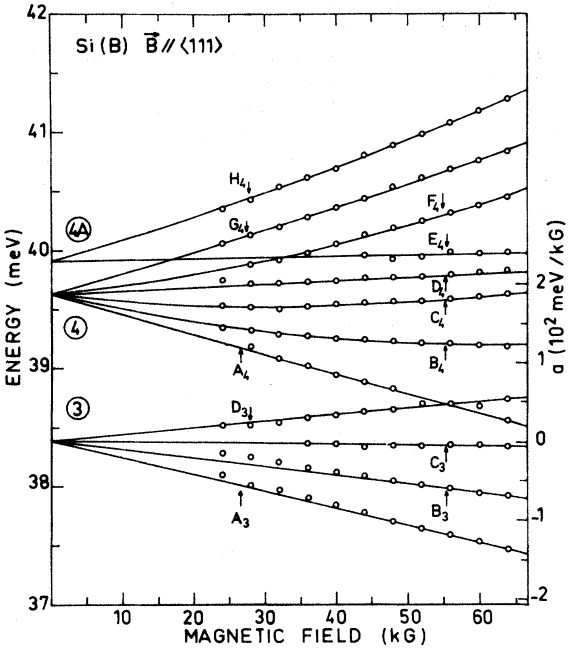

FIG. 14. Same as Fig. 5 for $\vec{E} \perp \vec{B} \parallel \langle 111 \rangle$.

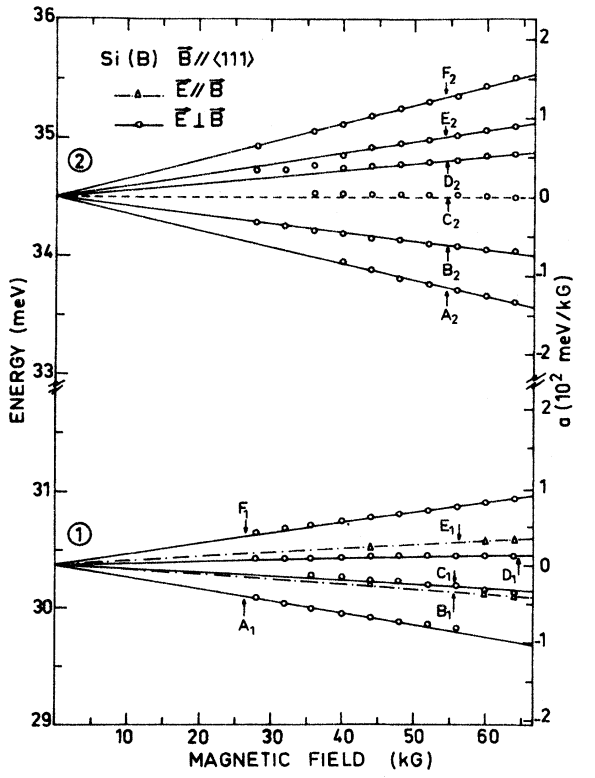

FIG. 13. Same as Fig. 4 for $\vec{B} \parallel \langle 111 \rangle$. For the component C_2^*, see the text.

explain qualitatively the splitting observed for $\vec{B} \parallel \langle 100 \rangle$; this is in contradiction with what is observed for $\vec{B} \parallel \langle 011 \rangle$ when the selection rules are taken into account.

The shifts of the centers of gravity observed for

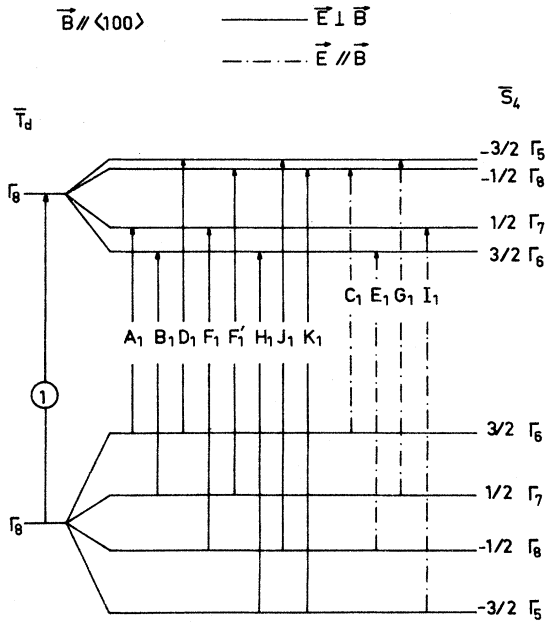

FIG. 15. Proposed energy-level scheme for line 1 when $\vec{B} \parallel \langle 100 \rangle$.

TABLE XIV. Assignment of the Zeeman components of line 1 observed for $\vec{B} \parallel \langle 100 \rangle$ to the allowed transitions between two $\Gamma_8(\frac{3}{2})$ levels. The splitting parameters predicted are obtained by using the experimental g factors of Table XVII. The effect of thermalization is not included in the calculation of the relative intensities.

Component $E_\perp$	Component $E_\parallel$	Transition	a_{pred} (10^2 meV/kG)	Relative intensity
A_1		$\frac{3}{2} \rightarrow \frac{1}{2}$	−1.34	0.10
B_1		$\frac{1}{2} \rightarrow \frac{3}{2}$	−0.92	0.10
	C_1	$\frac{3}{2} \rightarrow -\frac{1}{2}$	−0.71	0.25
D_1		$\frac{3}{2} \rightarrow -\frac{3}{2}$	−0.60	0.15
	E_1	$-\frac{1}{2} \rightarrow \frac{3}{2}$	−0.32	0.25
F_1		$-\frac{1}{2} \rightarrow \frac{1}{2}$	−0.06	0.15
F_1'		$\frac{1}{2} \rightarrow -\frac{1}{2}$	−0.03	0.15
	G_1	$\frac{1}{2} \rightarrow -\frac{3}{2}$	0.08	0.25
H_1		$-\frac{3}{2} \rightarrow \frac{3}{2}$	0.36	0.15
	I_1	$-\frac{3}{2} \rightarrow \frac{1}{2}$	0.62	0.25
J_1		$-\frac{1}{2} \rightarrow -\frac{3}{2}$	0.68	0.10
K_1		$-\frac{3}{2} \rightarrow -\frac{1}{2}$	1.25	0.10

line 2 are positive and this allows us to eliminate the possibility of an asymmetric splitting of the ground state combined with a symmetric splitting of the excited state. The data pertinent to that line are summarized in Table XXI.

C. Line 3

This line is much weaker than lines 1 and 2 and the relative intensities of the components can be

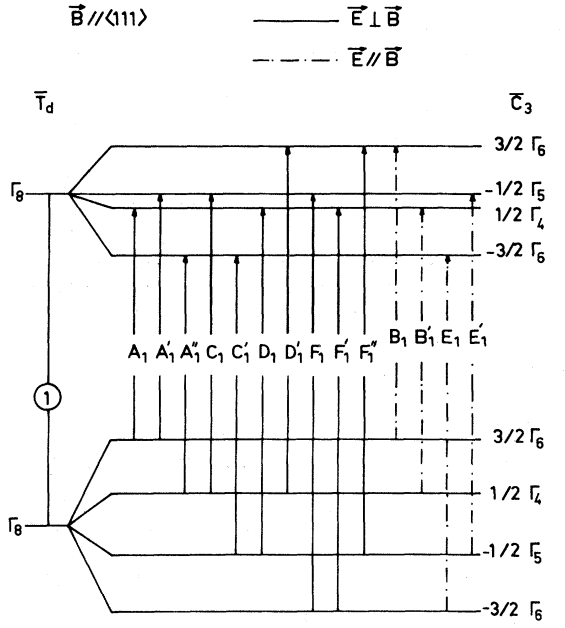

FIG. 16. Proposed energy-level scheme for line 1 when $\vec{B} \parallel \langle 111 \rangle$. The two transitions corresponding to $\Delta m_J = \pm 3$ are not indicated.

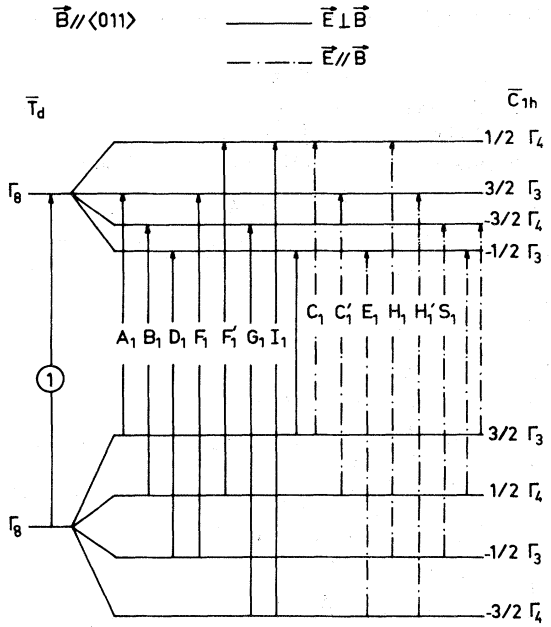

FIG. 17. Proposed energy-level scheme for line 1 when $\vec{B} \parallel \langle 011 \rangle$. The unlabeled transitions are not observed.

modified in the vicinity of lines 4 and 4A, so that their use as a guide to the assignment of the observed Zeeman component to specific transitions is not considered reliable. For $\vec{B} \parallel \langle 100 \rangle$, a level

TABLE XV. Assignment of the Zeeman components of line 1 observed for $\vec{B} \parallel \langle 111 \rangle$ to the allowed transitions between two $\Gamma_8(\frac{3}{2})$ levels. The predicted values of the splitting parameters are obtained by using the experimental g factors of Table XVII. The effect of thermalization is not included in the calculation of the relative intensities.

Component $E_\perp$	Component $E_\parallel$	Transition	a_{pred} (10^2 meV/kG)	Relative intensity
A_1		$\frac{3}{2} \rightarrow \frac{1}{2}$	−1.13	0.08
A_1'		$\frac{3}{2} \rightarrow -\frac{1}{2}$	−0.98	0.07
A_1''		$\frac{1}{2} \rightarrow -\frac{3}{2}$	−0.99	0.08
	B_1	$\frac{3}{2} \rightarrow \frac{3}{2}$	−0.44	0.40
	B_1'	$\frac{1}{2} \rightarrow \frac{1}{2}$	−0.51	0.05
C_1		$\frac{1}{2} \rightarrow -\frac{1}{2}$	−0.36	0.20
C_1'		$-\frac{1}{2} \rightarrow -\frac{3}{2}$	−0.30	0.07
D_1		$-\frac{1}{2} \rightarrow \frac{1}{2}$	0.18	0.20
D_1'		$\frac{1}{2} \rightarrow \frac{3}{2}$	0.18	0.07
	E_1	$-\frac{3}{2} \rightarrow -\frac{3}{2}$	0.32	0.40
	E_1'	$-\frac{1}{2} \rightarrow -\frac{1}{2}$	0.33	0.05
F_1		$-\frac{3}{2} \rightarrow -\frac{1}{2}$	0.80	0.08
F_1'		$-\frac{3}{2} \rightarrow \frac{1}{2}$	0.95	0.07
F_1''		$-\frac{1}{2} \rightarrow \frac{3}{2}$	0.87	0.08
	...	$\frac{3}{2} \rightarrow \frac{3}{2}$	−1.61	0.05
	...	$-\frac{3}{2} \rightarrow \frac{3}{2}$	1.49	0.05

TABLE XVI. Assignment of the Zeeman components of line 1 observed for $\vec{B} \parallel \langle 011 \rangle$ to the allowed transitions between two $\Gamma_8(\frac{3}{2})$ levels. The predicted values are obtained by using the experimental g factors of Table XVII. The relative intensities do not include the effect of thermalization, and for the $E_\perp$ components, they correspond to $\vec{B} \parallel [110]$, $\vec{E} \parallel [\bar{1}10]$.

Component $E_\perp$	Component $E_\parallel$	Transition	a_{pred} (10^2 meV/kG)	Relative intensity
A_1		$\frac{3}{2} \rightarrow \frac{3}{2}$	-0.96	0.07
B_1		$\frac{1}{2} \rightarrow -\frac{3}{2}$	-0.66	0.35
	C_1	$\frac{3}{2} \rightarrow \frac{1}{2}$	-0.41	0.35
	C_1'	$\frac{1}{2} \rightarrow \frac{3}{2}$	-0.32	0.03
D_1		$-\frac{1}{2} \rightarrow -\frac{1}{2}$	-0.27	0.05
	S_1[a]	$-\frac{1}{2} \rightarrow -\frac{3}{2}$	0.02	0.03
	E_1	$-\frac{3}{2} \rightarrow -\frac{1}{2}$	0.36	0.35
F_1		$-\frac{1}{2} \rightarrow \frac{3}{2}$	0.35	0.35
F_1'		$\frac{1}{2} \rightarrow \frac{1}{2}$	0.24	0.05
G_1		$-\frac{3}{2} \rightarrow -\frac{3}{2}$	0.65	0.07
	H_1	$-\frac{1}{2} \rightarrow \frac{1}{2}$	0.98	0.07
	H_1'	$-\frac{3}{2} \rightarrow \frac{3}{2}$	0.90	0.05
I_1		$-\frac{3}{2} \rightarrow \frac{1}{2}$	1.53	0.03
...		$\frac{3}{2} \rightarrow -\frac{1}{2}$	-1.58	0.03
	...	$\frac{3}{2} \rightarrow -\frac{3}{2}$	-0.13	0.05
	...	$\frac{1}{2} \rightarrow -\frac{1}{2}$	-0.93	0.07

[a]Observed as a shoulder on the low-energy side of E_1.

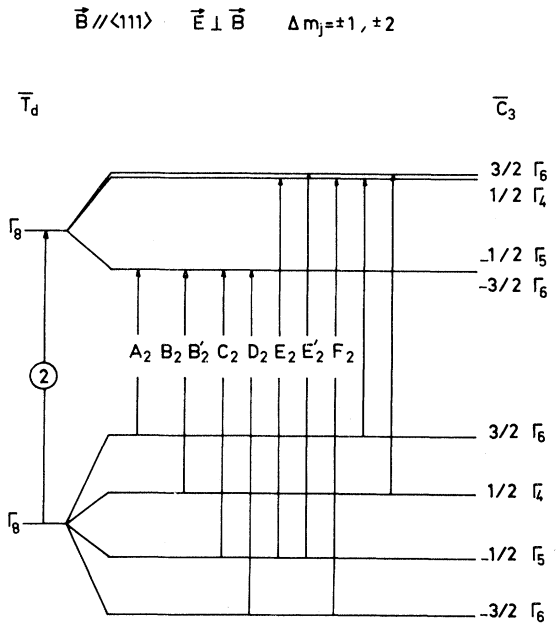

FIG. 19. Proposed energy-level scheme for line 2 when $\vec{B} \parallel \langle 111 \rangle$. The unlabeled transitions are not observed, the transitions corresponding to $\Delta m_j = 0, \pm 3$, observed for $\vec{E} \parallel \vec{B}$, are not indicated.

scheme which allows for the components observed is shown in Fig. 21 for a magnetic field of 66.67 kG The strong A_3 component arises from a $\frac{1}{2} \rightarrow \frac{3}{2}$ transition and the C_3 component from the $\frac{3}{2} \rightarrow -\frac{3}{2}$ transition, but the component which should be associated with the $-\frac{3}{2} \rightarrow \frac{3}{2}$ component is not observed. The D_3 component is the superposition of the $-\frac{1}{2} \rightarrow \frac{1}{2}$ and $\frac{1}{2} \rightarrow -\frac{1}{2}$ transitions. The components C_3 and F_3 exhibit approximately the same negative quadratic shift which is consistent with their assignment and indicate a repulsion of the upper sublevels of the excited state of line 3.

This level scheme is tentative; it shows the same ordering and the same tendency as for line 1, but we did not try to calculate the g factors and the anisotropy parameter as the excited levels of line 3 interact with that of line 4, resulting in a small negative shift for some of the observed components.

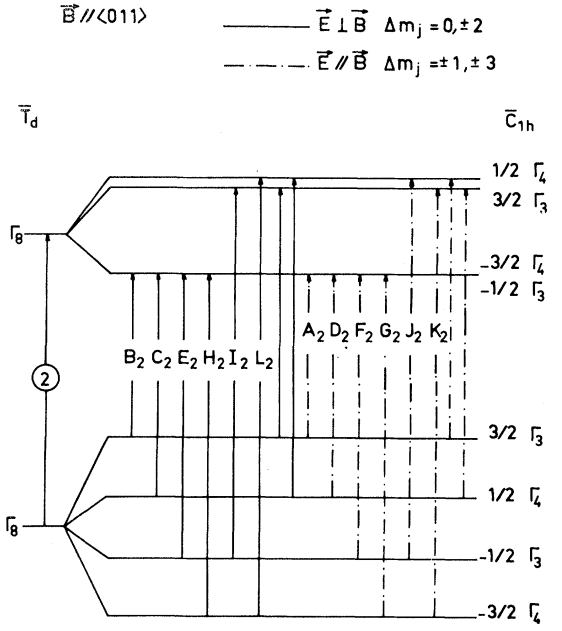

FIG. 18. Same as Fig. 17 for line 2.

TABLE XVII. g factors of the ground and excited states of line 1. The calculated values are obtained by using the experimental data for $\vec{B} \parallel \langle 100 \rangle$. The shifts are expressed in 10^3 meV/kG.

$\gamma = 0.010 \pm 0.003$ $g_1' = 1.03 \pm 0.07 = K$		$\gamma_1 = -0.056 \pm 0.008$ $g_1'(1) = -1.16 \pm 0.06 = K_1$	
	$\langle 100 \rangle$	$\langle 111 \rangle$	$\langle 011 \rangle$
$g_{1/2}$	1.04 ± 0.06	1.19 ± 0.08	1.13 ± 0.08
$g_{3/2}$	1.12 ± 0.02	1.11 ± 0.03	1.11 ± 0.03
$g_{1/2}(1)$	-1.09 ± 0.05	-0.26 ± 0.10	2.02 ± 0.10
$g_{3/2}(1)$	-0.57 ± 0.04	0.67 ± 0.04	0.19 ± 0.03
$(g_{1/2})_{\text{cal}}$		1.16	1.13
$(g_{3/2})_{\text{cal}}$		1.11	1.11
$(g_{1/2}(1))_{\text{cal}}$		-0.31	1.95
$(g_{3/2}(1))_{\text{cal}}$		0.67	0.19
$s_{\pm 1/2}(1)$	-0.5	-0.9	-0.3
$s_{\pm 3/2}(1)$	-1.2	-0.6	-1.7

TABLE XVIII. Assignment of the Zeeman components of line 2 observed for $\vec{B} \parallel \langle 011 \rangle$ to the allowed transitions between two $\Gamma_8(\frac{3}{2})$ levels. The predicted splitting parameters are obtained by using the experimental g factors of Table XXI.

Component $E_\perp$	Component $E_\parallel$	Transition	a_{pred} (10^2 meV/kG)
	A_2	$\frac{3}{2} \rightarrow -\frac{3}{2}$	−1.38
B_2		$\frac{3}{2} \rightarrow -\frac{1}{2}$	−1.38
C_2		$\frac{1}{2} \rightarrow -\frac{3}{2}$	−0.74
	D_2	$\frac{1}{2} \rightarrow -\frac{1}{2}$	−0.74
E_2		$-\frac{1}{2} \rightarrow -\frac{1}{2}$	−0.08
	F_2	$-\frac{1}{2} \rightarrow -\frac{3}{2}$	−0.08
	G_2	$-\frac{3}{2} \rightarrow -\frac{1}{2}$	0.56
H_2		$-\frac{3}{2} \rightarrow -\frac{3}{2}$	0.56
I_2		$-\frac{1}{2} \rightarrow \frac{3}{2}$	0.86
	J_2	$-\frac{1}{2} \rightarrow \frac{1}{2}$	0.96
	K_2	$-\frac{3}{2} \rightarrow \frac{3}{2}$	1.49
L_2		$-\frac{3}{2} \rightarrow \frac{1}{2}$	1.59
...		$\frac{3}{2} \rightarrow \frac{3}{2}$	−0.45
	...	$\frac{3}{2} \rightarrow \frac{1}{2}$	−0.35
	...	$\frac{1}{2} \rightarrow \frac{3}{2}$	0.20
...		$\frac{1}{2} \rightarrow \frac{1}{2}$	0.30

The same fitting has been made for $\vec{B} \parallel \langle 011 \rangle$ (Fig. 22) and $\vec{B} \parallel \langle 111 \rangle$. In the second case, noting the similarity between the linear splitting parameters of the low-energy components of line 2, the experimental data can be fitted to a degenerate $\{-\frac{1}{2}, -\frac{3}{2}\}$ excited sublevel; we do not know, however, whether the similarity is pure coincidence or it reflects a partial similarity which could appear for $\vec{B} \parallel \langle 111 \rangle$ because of a smaller interaction with the other excited states for that geometry. We cannot answer this question as long as we have no detailed description of the excited acceptor states. In Fig. 23 is given a second possibility which explains the splitting of line 3 for $\vec{B} \parallel \langle 111 \rangle$, but the number of components observed is insufficient to make a choice. We have also considered the possibility for line 3 to be due to a transition to a level with symmetry $\Gamma_6 + \Gamma_7$, but this leads to impossibilities in the interpretation of the spectra with the selection rules of Table II.

TABLE XIX. Assignment of the Zeeman components of line 2 observed for $\vec{B} \parallel \langle 111 \rangle$ to the allowed $E_\perp$ transitions between two $\Gamma_8(\frac{3}{2})$ sublevels. The predicted splitting parameters are obtained by using the experimental g factors of Table XXI.

Component	Transition	a_{pred} (10^2 meV/kG)
A_2	$\frac{3}{2} \rightarrow -\frac{1}{2}$	−1.37
B_2	$\frac{1}{2} \rightarrow -\frac{3}{2}$	−0.75
B_2'	$\frac{1}{2} \rightarrow -\frac{1}{2}$	−0.75
C_2'	$-\frac{1}{2} \rightarrow -\frac{3}{2}$	−0.06
D_2	$-\frac{3}{2} \rightarrow -\frac{1}{2}$	0.56
E_2	$-\frac{1}{2} \rightarrow \frac{1}{2}$	0.98
E_2'	$-\frac{1}{2} \rightarrow \frac{3}{2}$	0.93
F_2	$-\frac{3}{2} \rightarrow \frac{1}{2}$	1.55
...	$\frac{3}{2} \rightarrow \frac{1}{2}$	0.08
...	$\frac{1}{2} \rightarrow \frac{3}{2}$	0.73

TABLE XX. Assignment of the Zeeman components of line 2 observed for $\vec{B} \parallel \langle 100 \rangle$ to the allowed transitions between two $\Gamma_8(\frac{3}{2})$ sublevels. The predicted splittings are obtained by using the experimental g factors of Table XXI.

Component $E_\perp$	Component $E_\parallel$	Transition	a_{pred} (10^2 meV/kG)
A_2		$\frac{3}{2} \rightarrow \frac{1}{2}$	−1.32
A_2'		$\frac{3}{2} \rightarrow -\frac{3}{2}$	−1.44
	B_2	$\frac{1}{2} \rightarrow -\frac{3}{2}$	−0.65
	C_2	$\frac{3}{2} \rightarrow -\frac{1}{2}$	−0.36
D_2		$-\frac{1}{2} \rightarrow \frac{1}{2}$	−0.17
D_2'		$-\frac{1}{2} \rightarrow -\frac{3}{2}$	−0.05
D_2''		$\frac{1}{2} \rightarrow \frac{3}{2}$	0.27
D_2'''		$\frac{1}{2} \rightarrow -\frac{1}{2}$	0.32
	E_2	$-\frac{3}{2} \rightarrow \frac{1}{2}$	0.51
	E_2'	$-\frac{1}{2} \rightarrow \frac{3}{2}$	0.87
F_2		$-\frac{3}{2} \rightarrow \frac{3}{2}$	1.55
F_2'		$-\frac{3}{2} \rightarrow -\frac{1}{2}$	1.59

D. Line 4

The symmetry of the excited state of line 4 has been found to be a combination $\Gamma_6 + \Gamma_7$ of the point

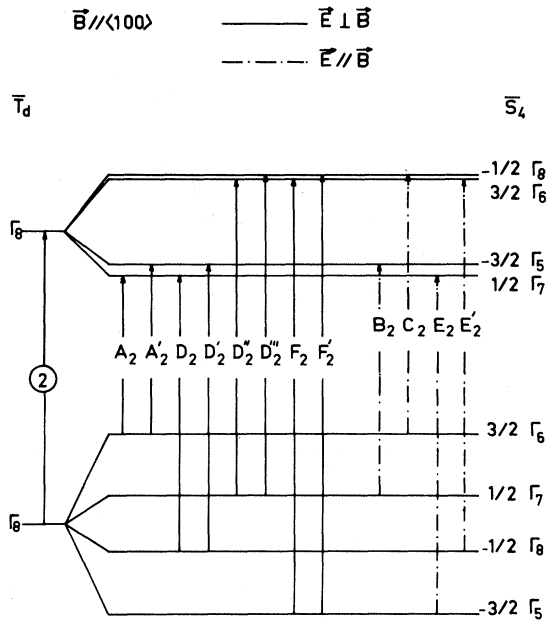

FIG. 20. Proposed level scheme for line 2 when $\vec{B} \parallel \langle 100 \rangle$.

TABLE XXI. g factors of the excited state of line 2. The calculated values are obtained by using $g_1'(2)$ and r_2 deduced from the experimental data for $\vec{B} \parallel \langle 011 \rangle$. The shifts are expressed in 10^3 meV/kG.

	$g_1'(2) = -2.17 \pm 0.76$	$r_2 = -0.137 \pm 0.008$	
	$\langle 100 \rangle$	$\langle 111 \rangle$	$\langle 011 \rangle$
$g_{1/2}(2)$	-1.86 ± 0.16	1.71 ± 0.16	1.79 ± 0.13
$g_{3/2}(2)$	0.53 ± 0.05	0.60 ± 0.05	0.54 ± 0.04
$[g_{1/2}(2)]_{cal}$	-1.87	1.70	
$[g_{3/2}(2)]_{cal}$	0.51	0.57	
$s_{\pm 1/2}(2)$	0.8	0.8	0.11
$s_{\pm 3/2}(2)$	1.2	0.11	0.05

group $\overline{T}_d$ by observing the polarization features of the components of this line when split by a uniaxial stress.[29] It must be reminded that, in the absence of perturbation, the quadratic shift must be the same for the two sublevels associated with $|m_j|$, and that for Γ_6 and Γ_7 levels, the shifts and the g factors are isotropic.

For $\vec{B} \parallel \langle 100 \rangle$, we observe three $E_\parallel$ components whereas for a $\Gamma_8 - \Gamma_X$ transition, group theory predicts four components of this type, provided Γ_X is Γ_8, $2\Gamma_6$, $2\Gamma_7$, or $\Gamma_6 + \Gamma_7$. The assignment has been made on the basis of $\Gamma_X = \Gamma_6 + \Gamma_7$. Several possibilities have been investigated, but for all of them, we were unable, under reasonable assumptions, to locate more than three sublevels using the selection rules of Table II, the spacing between the components and the quadratic splitting parameters. We then obtain for a value of the magnetic field of 66.67 kG the level scheme of Fig. 21. Following our assignment, I_4 and J_4 should exhibit the same

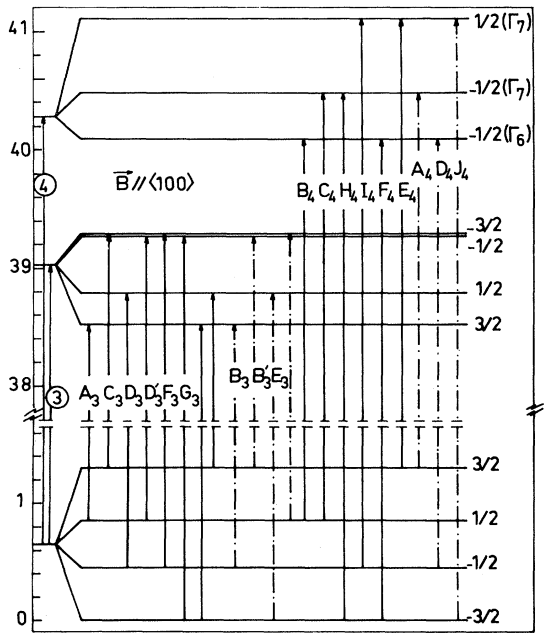

FIG. 21. Proposed energy-level scheme for lines 3 and 4 when $\vec{B} \parallel \langle 100 \rangle$. The energy scale is given in meV. The position of the levels corresponds to a field of 66.67 kG and the quadratic shift is included. The unlabeled components are not observed.

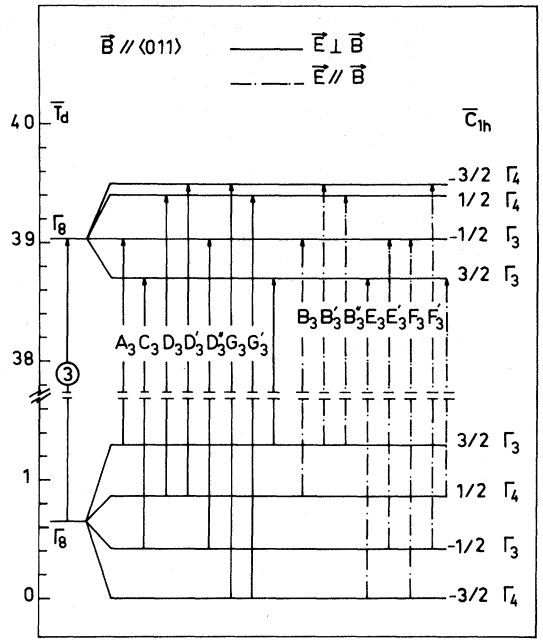

FIG. 22. Same as Fig. 21 for line 3 when $\vec{B} \parallel \langle 011 \rangle$.

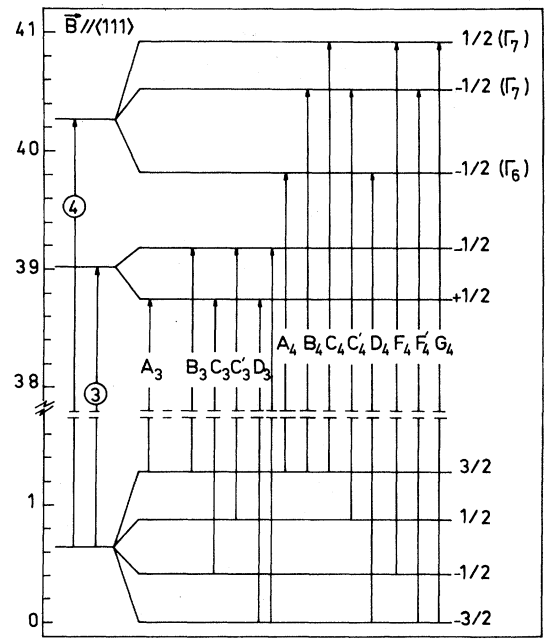

FIG. 23. Same as Fig. 21 when $\vec{E} \perp \vec{B} \parallel \langle 111 \rangle$.

quadratic shift but this is not the case. We believe that it is more realistic to adopt for the $\frac{1}{2}(\Gamma_7)$ sublevel the shift of the component J_4, as the observed position of the component I_4 can be slightly modified by the component H_4 and by the unlabeled component observed only for fields less than 52 kG. The agreement regarding $b(A_4)$ and $b(C_4)$ is good and comparable with $b(H_4)$, leading for $-\frac{1}{2}(\Gamma_7)$ to a shift of $(0.99 \pm 0.10) \times 10^{-4}$ meV/kG^2. The quadratic shift of the $-\frac{1}{2}(\Gamma_6)$ sublevel is taken as the average of $b(B_4)$ and $b(D_4)$ and it is about one-half that of the $-\frac{1}{2}(\Gamma_7)$ sublevels.

One can wonder why the position of the $\frac{1}{2}(\Gamma_6)$ sublevel cannot be determined. First, it is clear that the relations derived in Ref. 20 for the relative intensities of the transitions cannot be used in the case of lines 4 and 4A. If we consider for instance the relatively strong intensities of some components ascribed to line 4A, it is possible that the intensities of the transitions from the sublevels of Γ_8 to $\frac{1}{2}(\Gamma_6)$ are too weak to be detected. There can be also an accidental degeneracy at high field between $\frac{1}{2}(\Gamma_6)$ and $\frac{1}{2}(\Gamma_7)$. This does not modify the scheme of Fig. 21 for the $E_\perp$ transitions, but it adds a new $\frac{1}{2} \rightarrow \frac{1}{2}(\Gamma_6)$ transition which could be tentatively identified with the component G_4, this strong component being also associated with certainty with some transition to an excited sublevel of the line 4A. Under this assumption, one could attribute I_4 to the $-\frac{1}{2} \rightarrow \frac{1}{2}(\Gamma_6)$ transition and this could also explain why the shift of this line is so different from that of line J_4. By subtracting the quadratic contributions from the position of the levels given in Fig. 21, we obtain the linear splitting parameters of Table XXII, yielding $g_7(4) = 2.23 \pm 0.13$ and $g_6(4) = 2.25 \pm 0.14$ if we adopt a linear splitting of 0.0072 meV/kG for the $\frac{1}{2}(\Gamma_6)$ sublevel. The centers of gravity of the $\frac{1}{2}(\Gamma_6)$ and $\frac{1}{2}(\Gamma_7)$ components are 39.67 and 39.82 meV, respectively, showing that, under our assumption, the center of gravity of the $\frac{1}{2}(\Gamma_6)$ levels is not too distant from the zero-field position of line 4, but that the center of gravity of the $\frac{1}{2}(\Gamma_7)$ levels is nearer to line 4A than to line 4. We believe that this situation can reflect a strong high-field coupling between the sublevels of lines 4 and 4A for $\vec{B} \parallel \langle 100 \rangle$. The value obtained for $g_7(4)$ is of course independent of the above assumption.

The components observed for $\vec{B} \parallel \langle 111 \rangle$ can be fit to a three-level scheme similar to that obtained for $\vec{B} \parallel \langle 100 \rangle$, but we cannot decide without further discussion whether the excited sublevel of highest energy is $\frac{1}{2}(\Gamma_6)$ or $\frac{1}{2}(\Gamma_7)$ as the selection rules are the same in both cases, Fig. 23. This and the fact that the components C_4 and F_4 each are the superposition of two transitions complicate the analysis of the splitting. We take $b(B_4) = (1.15 \pm 0.06) \times 10^{-4}$ meV/kG^2 for the shift of $-\frac{1}{2}(\Gamma_7)$, as it is a "pure" shift, and $(0.12 \pm 0.06) \times 10^{-4}$ meV/kG^2 for the shift of $-\frac{1}{2}(\Gamma_6)$. The sublevel of highest energy must be $-\frac{1}{2}(\Gamma_6)$, $\frac{1}{2}(\Gamma_7)$ or both if we repeat the assumption made for $\vec{B} \parallel \langle 100 \rangle$. In the first case, $b(G_4) = (0.31 \pm 0.06) \times 10^4$ meV/kG^2 corresponds to the shift of either the $\frac{1}{2}(\Gamma_6)$ or the $\frac{1}{2}(\Gamma_7)$ sublevels and we deduce $g_6(4) = 2.59 \pm 0.13$ or $g_7(4) = 1.95 \pm 0.12$. The latter g factor corresponds to the ordering of the sublevels given in Table XXII. Under the hypothesis of the degeneracy of the two sublevels, several supplementary assumptions must be made to reach a conclusion. The simplest is that the shift of $\frac{1}{2}(\Gamma_6)$ is the same as that of $\frac{1}{2}(\Gamma_7)$, but this does not seem likely owing to the difference between the shifts of $-\frac{1}{2}(\Gamma_6)$ and $-\frac{1}{2}(\Gamma_7)$. It can be verified that if we assume the shift for $\frac{1}{2}(\Gamma_7)$ to be 0.90×10^{-4} meV/kG^2, which is not very different from the shift for $-\frac{1}{2}(\Gamma_7)$ and keep the shift for $-\frac{1}{2}(\Gamma_6)$ to 0.31×10^{-4} meV/kG^2, we obtain $g_6(4) = 2.62$ and $g_7(4) = 1.32$. The above assumption has been chosen only because with the g values obtained, it can be verified that the centers of gravity of the two Γ_6 and Γ_7 levels come very close to the zero-field position of line 4.

The assignment of the components for $\vec{B} \parallel \langle 011 \rangle$ has been made on the basis of the three-level scheme already obtained for $\vec{B} \parallel \langle 100 \rangle$ and $\vec{B} \parallel \langle 111 \rangle$

TABLE XXII. Linear splitting (lsp) parameters (10^2 meV/kG) and quadratic shifts (qs) (10^4 meV/kG^2) of the excited state of line 4 deduced from the level schemes of Figs. 21, 23, and 24. The splitting parameters of the ground state are also given for an estimation of the splitting of the various components.

	$\vec{B} \parallel \langle 100 \rangle$		$\vec{B} \parallel \langle 111 \rangle$		$\vec{B} \parallel \langle 011 \rangle$	
Level	lsp	qs	lsp	qs	lsp	qs
$\frac{1}{2}(\Gamma_7)$	0.93	0.47 ± 0.11	0.77	0.31 ± 0.06	0.59	1.06 ± 0.16
$-\frac{1}{2}(\Gamma_7)$	−0.36	0.99 ± 0.10	−0.36	1.15 ± 0.06	−0.44	0.57 ± 0.06
$-\frac{1}{2}(\Gamma_6)$	−0.57	0.43 ± 0.13	−0.75	0.12 ± 0.06	−0.65	0.35 ± 0.20
$\frac{3}{2}(g)$	0.98		0.96		0.97	
$\frac{1}{2}(g)$	0.30		0.35		0.33	
$-\frac{1}{2}(g)$	−0.30		−0.35		−0.33	
$-\frac{3}{2}(g)$	−0.98		−0.96		−0.97	

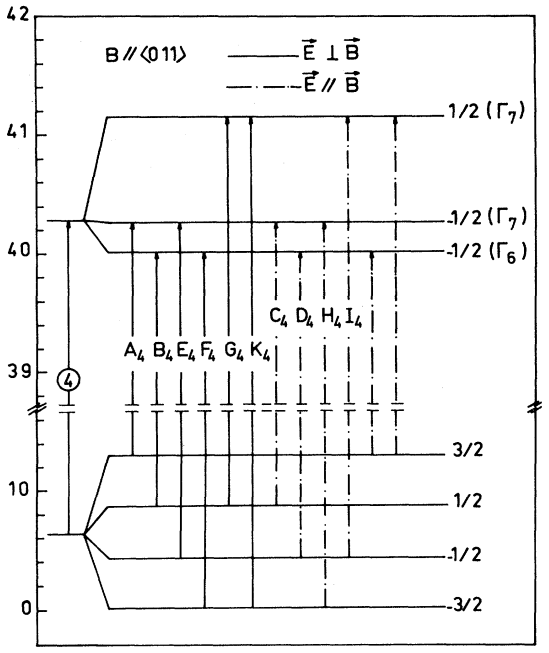

FIG. 24. Same as Fig. 21 for line 4 when $\vec{B} \parallel \langle 011 \rangle$.

as this scheme seems to fit well the experimental data (Fig. 24). There is no ambiguity for the shift of the $\frac{1}{2}(\Gamma_7)$ sublevel, found to be $(1.06 \pm 0.16) \times 10^{-4}$ meV/kG^2. There is, by contrast, an important difference between the shifts of the A_4 and H_4 components, but we are inclined to keep $b(A_4)$ for the shift of the $-\frac{1}{2}(\Gamma_7)$ sublevel, as A_4 is a relatively narrow component whereas H_4 can be modified by the neighboring components. The same argument leads us to prefer $b(B_4)$ to $b(D_4)$ to measure the shift of $-\frac{1}{2}(\Gamma_6)$. From this, we derive $g_7(4) = 1.77$ for $\vec{B} \parallel \langle 011 \rangle$, and this value should be compared to 2.23 and 1.95 obtained for $g_7(4)$ for $\vec{B} \parallel \langle 100 \rangle$ and $\vec{B} \parallel \langle 111 \rangle$, respectively, which support the fact that $g_7(4) \sim 2$.

Table XXII summarizes the results obtained for line 4. One can note that the relative magnitudes of the quadratic shifts of the Γ_7 sublevels are similar for $\vec{B} \parallel \langle 100 \rangle$ and $\vec{B} \parallel \langle 111 \rangle$, but there is an inversion for $\vec{B} \parallel \langle 011 \rangle$. The positions of some of the Zeeman sublevels deduced from this table differ slightly from those shown in Figs. 22 and 24 because of the correlation between the quadratic splitting parameters and the shift of the sublevels which is shown above. We cannot give with certainty a value for $g_6(4)$. We believe, however, from the discussion for $\vec{B} \parallel \langle 100 \rangle$ that a value of $g_6(4) \simeq g_7(4)$ does not look unrealistic.

VI. CONCLUSION

The discussion of the experimental results has provided some evidence and also raised some questions. First, it seems that the ground-state splitting is nearly isotropic but that a small anisotropy is detectable. We have obtained for $g_{1/2}(100)$ a value somewhat higher that that of Ref. 16 and from the convergence of our results we believe that $g_{1/2}(100)$ is nearer to 1.0 than to 0.9. We have assumed the splitting of the ground state to be symmetric within the accuracy of our results since we could not evaluate an asymmetry smaller than the zero-field linewidth. This is not in contradiction with the results of Ref. 15 because of the difference in the magnitude of the fields used in the two experiments. Nonetheless, we have observed at high field components with relatively small width (~0.10 meV) and that implies probably a maximum width of ~0.06 meV for the ground-state sublevels for a magnetic field of 64 kG in lightly doped specimens. An indirect determination of the g factor g_h of the hole has been done recently by Honig and Vanier, who have studied spin-polarization-dependent luminescence associated with electron transfer from phosphorus to boron impurities in silicon.[31] They obtained $g_h = 0.90^{+0.05}_{-0.10}$ for $\vec{B} \parallel \langle 111 \rangle$; and this is smaller than $g_{1/2}(111) = 1.19 \pm 0.09$ derived from our experiments or $g_i(111) = 1.26 \pm 0.04$ given in Ref. 16 on the basis of an isotropic model. On the other hand, it compares favorably with $g_i(100) = 0.88 \pm 0.06$ and $g_{1/2}(100) = 1.04 \pm 0.06$. It could be due to an overestimate of the strain effect included in the relation giving the field-dependent radiative recombination rate, used to fit the experimental luminescence spectra.

The determination of the g factors of the ground and excited states has been done under specific assumptions of the shifts of the centers of gravity of the sublevels with given $|m_j|$. We have not tried to elucidate their physical meaning but we think that they can be related for the excited states to the removing of the degeneracy of the $\Gamma_8^+(\frac{3}{2})$ valence band by the magnetic field. The splitting of line 1 has been successfully explained. The observed anisotropy of the splitting of the excited state of line 1 is also in agreement with theoretical predictions, and we have obtained an estimate of the parameters u_1 and v_1 governing the relative intensities of the Zeeman components, introduced in the group-theoretical analysis of Ref. 20. In contrast to the situation for boron in germanium, the reason for a near identity of the positions of the $E_\parallel$ and $E_\perp$ components is to be found only in the splitting of the excited states. The agreement in the assignment of the components of line 2 is not as good as for line 1 and a reason for this is the broadening of the Zeeman components, which prevents unambiguous assignment of the transitions. The results for line 3 are not thought to fit the analysis of Ref. 20 as well as those for lines 1 and 2 because of the proximity of lines 4 and 4A and because of uncertain-

ties inherent to the intensity of that line. It can be remarked that the maximum splittings of the excited states for lines 1, 2, and 3 (for $\vec{B} \parallel \langle 100 \rangle$) are not very different: they correspond to an average of 0.7 meV for a field of 64 kG, whereas the corresponding figure for the ground state is 1.3 meV. For line D of boron in germanium, the converse is qualitatively observed, with an average ratio of 0.25 between the maximum splitting of the ground and excited states, and the same ratio is ~8.4 for the Raman-active line of boron in silicon. The components of lines 4 and 4A exhibit a shift which cannot be explained by the repulsion of the components of line 3. We can correlate that with the fact that line 4 does not have a Γ_8 symmetry and that the same is also observed for the C line of boron in germanium. The Zeeman splitting of the $2p'$ line of the $p_{1/2}$ series of boron in silicon has been observed by Zwerdling *et al.* to resolve into a quadruplet for $\vec{E} \perp \vec{B} \parallel \langle 111 \rangle$. This line has been attributed to a $\Gamma_8 \rightarrow \Gamma_6$ transition. If we assume the two extreme components to be $-\frac{3}{2} \rightarrow \frac{1}{2}(\Gamma_6)$ or $-\frac{1}{2}(\Gamma_6)$ and $\frac{3}{2} \rightarrow -\frac{1}{2}(\Gamma_6)$ or $\frac{1}{2}(\Gamma_6)$, we obtain an apparent g factor whose magnitude is ~7. This is a fairly high value compared with the g factors of the levels of the $p_{3/2}$ series, but it reflects partially the Landau splitting of the valence band. A Zeeman study of indium in silicon would be useful in indicating the effect of the chemical nature of the impurity on the splitting of the acceptor level. For thallium in germanium, the difference is small, but in silicon the effect on the zero-field position of the acceptor ground states is already pronounced. The use of well-collimated infrared synchrotron radiation or of a quarter-wave plate made from thallium bromoiodide can allow measurements with circularly polarized radiation, and this can simplify the patterns and eliminate possibilities for $\vec{B} \parallel \langle 100 \rangle$ and $\vec{B} \parallel \langle 111 \rangle$.

ACKNOWLEDGMENTS

It is a pleasure to thank Dr. A. Honig for sending a report of his paper prior to publication. We wish to thank Dr. J. P. Bouchaud, from SILEC S.C., for providing the silicon crystals used for this study and to acknowledge the fine work done by Mr. Bertrand from CNET in the orientation and cutting of the samples.

[1] W. Kohn, *Solid State Physics*, edited by F. Seitz and D. Turnbull (Academic, New York, 1957), Vol. 5, p. 257.

[2] D. Schetcher, J. Phys. Chem. Solids 23, 237 (1962).

[3] K. S. Mendelson and H. M. James, J. Phys. Chem. Solids 25, 729 (1964).

[4] K. S. Mendelson and D. R. Schultz, Phys. Status Solidi 31, 59 (1969).

[5] A. Baldereschi and N. O. Lipari, Phys. Rev. B 9, 1525 (1974).

[6] R. A. Faulkner, Phys. Rev. 184, 713 (1969).

[7] P. Fisher and A. K. Ramdas, *Physics of the Solid State*, edited by S. Balakrishna, M. Krishnamurthi, and B. Ramachandra Rao (Academic, New York, 1969), p. 149.

[8] H. R. Chandrasekhar, P. Fisher, A. K. Ramdas, and S. Rodriguez, Phys. Rev. B 8, 3836 (1973).

[9] S. Zwerdling, K. J. Button, and B. Lax, Phys. Rev. 118, 975 (1960).

[10] S. Zwerdling, K. J. Button, B. Lax, and L. M. Roth, Phys. Rev. Lett. 4, 173 (1960).

[11] W. J. Moore, J. Phys. Chem. Solids 32, 93 (1971).

[12] H. P. Soepangkat and P. Fisher, Phys. Rev. B 8, 870 (1973).

[13] K. Suzuki, M. Okazaki, and H. Hasegawa, J. Phys. Soc. Jpn. 19, 930 (1964).

[14] P. J. Lin-Chung and R. F. Wallis, J. Phys. Chem. Solids 30, 1453 (1969).

[15] G. Feher, J. C. Hensel, and E. A. Gere, Phys. Rev. Lett. 5, 309 (1960).

[16] J. M. Cherlow, R. L. Aggarwal, and B. Lax, Phys. Rev. B 7, 4547 (1973).

[17] K. Colbow, Can. J. Phys. 41, 1801 (1963).

[18] B. Bleaney, Proc. Phys. Soc. Lond. 73, 939 (1959).

[19] Y. Yafet and D. G. Thomas, Phys. Rev. 131, 2405 (1963).

[20] A. K. Bhattacharjee and S. Rodriguez, Phys. Rev. B 6, 3836 (1972).

[21] G. L. Bir, E. I. Butikov, and G. E. Pikus, J. Phys. Chem. Solids 24, 1467 (1963).

[22] Manufactured by Perkin Elmer Ltd., Beaconsfield, Bucks, England.

[23] Model IGP 223 polarizer from AIM Physical Sciences, Cambridge, England.

[24] K. N. Rao, W. W. Brim, V. L. Sinnet, and R. H. Wilson, J. Opt. Soc. Am. 52, 862 (1962).

[25] M. M. Randall, D. M. Dennison, N. Ginsburg, and L. R. Weber, Phys. Rev. 52, 160 (1937).

[26] Manufactured by Oxford Instruments, Oxford, England.

[27] S. D. Smith, in *Encyclopedia of Physics*, edited by L. Genzel (Springer, New York, 1967), Vol. XXV/2a, p. 234.

[28] G. Taravella, Ph. Arcas, and B. Pajot, Solid State Commun. 13, 353 (1973).

[29] A. Onton, P. Fisher, and A. K. Ramdas, Phys. Rev. 163, 686 (1967).

[30] H. R. Chandrasekhar, Ph.D. thesis (Purdue University, 1974) (unpublished).

[31] A. Honig and P. E. Vanier, in *Proceedings of the Twelfth Conference on the Physics of Semiconductors*, edited by M. H. Pilkhun (Teubner, Stuttgart, 1974), p. 751.